Control Strategies of Three-Phase Distributed Generation Inverters for Grid Unbalanced Voltage Compensation

Farzam Nejabatkhah, *Student Member, IEEE*, Yun Wei Li, *Senior Member, IEEE*, and Bin Wu, *Fellow, IEEE*

***Abstract*—The high penetration level of power electronics interfaced distributed generation (DG) systems creates great ancillary services potential through the DG interfacing converters, such as the grid unbalanced voltage compensation. However, the unbalanced voltage compensation may cause adverse effects on the DGs' operation, such as output active power oscillation and dc-link voltage variations. Moreover, since the compensation is realized through the available rating of DGs' interfacing converters, it is equally important to consider the effectiveness of control strategy for unbalanced voltage compensation. Considering these challenging issues, two grid unbalanced voltage compensation strategies for three-phase power electronics interfaced DG systems are proposed in this paper. Especially, the first control strategy aims at minimizing the DG's active power oscillation and reducing the adverse effects of unbalanced voltage compensation on DG's operation. The second control strategy focuses on the effectiveness of unbalanced voltage compensation by controlling DG's negative sequence current to be inphase with the grid negative sequence current. Performances of the two proposed control strategies under different grid conditions and DG operating conditions are studied, and recommendations for appropriate control strategy utilization under various conditions are provided. Finally, validity of the proposed strategies is verified by both simulations and experimental results.**

***Index Terms*—Distributed generation (DG), negative sequence active and reactive powers, negative sequence voltage reduction, power oscillation minimization, unbalanced voltage compensation.**

I. Introduction

In recent years, distributed generations (DGs) that can be classified into power generation from renewable energy resources such as wind, photovoltaic, the clean alternative energy generation technologies such as fuel cells and microturbines, as well as the traditional rotational machine-based technologies, such as diesel generators, are playing an important role in active distribution or even transmission power systems [1]. In such systems with more interfacing power electronics from the DGs and loads, together with the increasing nonlinear loads, power quality will be an important topic. Among various power quality issues, unbalanced voltage caused by nonlinear loads, unbalanced loads, single-phase generators, and remote grid faults is one of the important issues of power quality, which causes adverse effects on the power system and equipment, such as electrical machine overheating, transformer overloading, capacity limitation of power electronics devices, more losses and less stability of power system, and negative impacts on induction motors and adjustable speed drives [2], [3].

In addition to aforementioned adverse effects of unbalanced voltage on the power system, unbalanced voltage causes double-frequency power oscillations at the output of power electronic converters, which are reflected as ripple in the dc-link voltage. This is particularly true considering that the dc-link capacitors in three-phase power systems are typically small. These oscillations in some cases lead to instability or system protection if the dc bus voltage exceeds the maximum limit. Moreover, unbalanced voltage will increase the peak current of power converters in the same active and reactive power production, which may result in over currents protection. Therefore, the unbalanced voltage concerns will lead the next generation of grid codes to consider the voltage support control in the steady state and transient operation [4], and appropriate methods should be applied in the distribution system in order to compensate the unbalanced voltage.

In general, the unbalanced voltage can be compensated using series active power filter by injecting negative sequence voltage [5], [6], shunt active power filter by injecting negative sequence current [7], [8], series–parallel compensators, such as unified power quality conditioner by injecting negative sequence voltage with series converter and negative sequence current with parallel converter [9], and static synchronous compensators by injecting positive and negative sequence reactive powers [2], [10], [11]. However, installing these additional equipment may increase the total investment cost.

With the increasing penetration of power electronics interfaced DGs, they can be properly controlled to help address the power quality issues and support the grid in addition to their power management targets. This is a promising idea since most interfacing converters are not operating at full rating all the time due to the intermittent nature of renewable energy sources. Therefore, the available converters rating can be used in a smart way to help improve the unbalanced voltage.

The control strategies of power electronics interfaced DGs under unbalanced voltage can be studied in two groups. In the

Manuscript received February 24, 2015; revised May 8, 2015; accepted September 11, 2015. Date of publication September 17, 2015; date of current version January 28, 2016. This work was supported in part by the Natural Sciences and Engineering Research Council of Canada and the State Key Lab of Power Systems (SKLD14KZ02), Tsinghua University. This paper was presented in part at the *IEEE Energy Conversion Congress and Exposition*, Montreal, ON, Canada, September 20–24, 2015. Recommended for publication by Associate Editor B. Wang.

F. Nejabatkhah and Y. W. Li are with the Department of Electrical and Computer Engineering, University of Alberta, Edmonton, AB T6G 2V4 Canada (e-mail: nejabatk@ualberta.ca; yunwei.li@ualberta.ca).

B. Wu is with the Department of Electrical and Computer Engineering, Ryerson University, Toronto, ON M5B 2K3 Canada (e-mail: bwu@ee.ryerson.ca).

Color versions of one or more of the figures in this paper are available online at http://ieeexplore.ieee.org.

Digital Object Identifier 10.1109/TPEL.2015.2479601

first group, control strategies only protect power converters from adverse effects of unbalanced voltage by canceling out output power oscillations and dc-link ripple [12]–[16]. In these control strategies, since the positive and negative sequence active and reactive powers are not controllable, the level of unbalanced voltage compensation cannot be adjusted. Moreover, active power oscillation cancellation may cause large peak current in converter output. In these strategies, the peak current of power electronic interfaced DGs can be controlled using average active and reactive powers control [15], [16]. In the second group, control strategies are focusing on adjustable unbalanced voltage compensation [17]–[23]. These control strategies, which are based on symmetric sequences, control interfacing converters' output positive and negative sequence active powers [18], positive and negative sequence reactive powers [19], [20] or positive and negative sequence active and reactive powers [15], [21], [22] for unbalanced voltage compensation. Although these control strategies sacrifice the interfacing converter local power quality problems (output power oscillations, dc-link ripples, and peak current enhancement), some of these problems have been considered. For example, unbalanced voltage compensation has been considered together with peak current control in [15], [18], and [21], while output active power oscillation control has been considered in [15] and [23]. However, these control strategies do not address all unbalanced voltage adverse effects on power electronic interfaced DG together with adjustable compensation at the same time. In addition, as the unbalanced voltage compensation is based on converter's available power rating, it is also important to design control strategies that can compensate the unbalanced ac voltage effectively.

In this paper, two control strategies for power electronics interfaced DGs are proposed in order to compensate the grid steady-state unbalanced voltage caused by unbalance loads. Both proposed methods are based on the DG's equivalent negative sequence virtual impedance amplitude and phase angle control. In the first strategy, DG's active power oscillation is minimized in order to reduce the adverse effects of compensation on the DG's operation. This method is named as active power oscillation minimization in this paper. In the second strategy, an effective method for reducing the negative sequence voltage of the grid is proposed, in which the DG's injected negative sequence current is controlled to be in the same phase with the grid negative sequence current. This method is named as inphase current compensation in this paper. In this paper, performances of the two proposed control strategies under different grid conditions in terms of $X_{\rm Grid}/R_{\rm Grid}$ ratios and different DG's operating conditions in terms of P/Q ratios are studied.

II. Principles of Instantaneous Power Theory

Fig. 1 shows the grid-connected DG through a three-phase voltage source inverter. The inverter is connected to the grid at the point of common coupling (PCC) with the LCL filter, and a three-phase unbalance load is connected to the PCC.

According to instantaneous power theory [16], [17], DG's instantaneous active and reactive powers injected into the grid

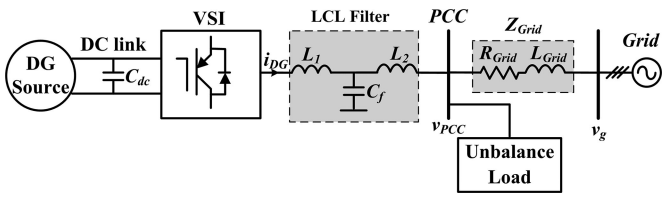

Fig. 1. Grid-connected DG power system.

are described as follows:

$$p_{\rm DG} = v_{\rm PCC} \cdot i_{\rm DG} \tag{1}$$

$$q_{\rm DG} = v_{\rm PCC_\perp} \cdot i_{\rm DG} \tag{2}$$

where $v_{\rm PCC} = [v_a, v_b, v_c]$ and $i_{\rm DG} = [i_a, i_b, i_c]^T$ are three-phase PCC voltage vector and the DG's output current vector, and $v_{\rm PCC_\perp}$ lags $v_{\rm PCC}$ by 90°. Considering symmetric-sequence component of the PCC voltage vector and the DG's output current vector, (1) and (2) are described as

$$\begin{aligned} p_{\rm DG} &= \left(v^+_{\rm PCC} + v^-_{\rm PCC}\right) \cdot \left(i^+_{\rm DG} + i^-_{\rm DG}\right) \\ &= \left(\underbrace{v^+_{\rm PCC} \cdot i^+_{\rm DG}}_{P^+_{\rm DG}} + \underbrace{v^-_{\rm PCC} \cdot i^-_{\rm DG}}_{P^-_{\rm DG}}\right) + \left(\underbrace{v^+_{\rm PCC} \cdot i^-_{\rm DG} + v^-_{\rm PCC} \cdot i^+_{\rm DG}}_{\tilde{p}_{\rm DG}}\right) \\ &= P_{\rm DG} + \tilde{p}_{\rm DG} \end{aligned} \tag{3}$$

$$\begin{aligned} q_{\rm DG} &= (v^+_{\rm PCC\perp} + v^-_{\rm PPC\perp}) \cdot (i^+_{\rm DG} + i^-_{\rm DG}) \\ &= \left(\underbrace{v^+_{\rm PCC\perp} \cdot i^+_{\rm DG}}_{Q^+_{\rm DG}} + \underbrace{v^-_{\rm PCC\perp} \cdot i^-_{\rm DG}}_{Q^-_{\rm DG}}\right) \cdot \left(\underbrace{v^+_{\rm PCC\perp} \cdot i^-_{\rm DG} + v^-_{\rm PCC\perp} \cdot i^+_{\rm DG}}_{\tilde{q}_{\rm DG}}\right) \\ &= Q_{\rm DG} + \tilde{q}_{\rm DG} \end{aligned} \tag{4}$$

where $v^+_{\rm PCC}$, $v^-_{\rm PCC}$, $i^+_{\rm DG}$, *and* $i^-_{\rm DG}$ are positive and negative sequence vector components of the three-phase PCC voltage vector and DG's output current vector, $P_{\rm DG}$ and $\tilde{p}_{\rm DG}$ are average and oscillatory terms of instantaneous active power, $P^+_{\rm DG}$ and $P^-_{\rm DG}$ are the positive and negative sequences of DG's average active power, Q and $\tilde{q}$ are average and oscillatory terms of instantaneous reactive power, and $Q^+_{\rm DG}$ and $Q^-_{\rm DG}$ are the positive and negative sequences of DG's average reactive power, respectively.

According to (3) and (4), the current vector that is aligned with voltage vector will generate active power, while the current vector that is aligned with orthogonal voltage vector will generate reactive power. Therefore, total DG's reference current vector considering symmetric-sequence components could be expressed as follows:

$$i_{\rm DG_{ref}} = \underbrace{a^+ v^+_{\rm PCC} + a^- v^-_{\rm PCC}}_{i_{\rm DG_P}} + \underbrace{b^+ v^+_{\rm PCC_\perp} + b^- v^-_{\rm PCC_\perp}}_{i_{\rm DG_q}} \tag{5}$$

where

$$a^+ = \frac{P_{\rm DG}}{\left|v^+_{\rm PCC}\right|^2},\ a^- = \frac{P_{\rm DG}}{\left|v^-_{\rm PCC}\right|^2},\ b^+ = \frac{Q_{\rm DG}}{\left|v^+_{\rm PCC}\right|^2},$$

and

$$b^{-} = \frac{Q_{\mathrm{DG}}}{\left|v^{-}_{\mathrm{PCC}}\right|^2}$$

are positive and negative sequence instantaneous conductances and susceptances. In the condition that injection of both positive and negative sequence active and reactive powers into the grid is desired, both sequences should be regulated to keep reference active and reactive powers constant. As a result, weighting factors k_1 and k_2 are defined as $k_1 = \frac{P^{+}_{\mathrm{DG}}}{P_{\mathrm{DG}}}$ and $k_2 = \frac{Q^{+}_{\mathrm{DG}}}{Q_{\mathrm{DG}}}$ to regulate the proportions of each sequence power delivered into the grid as follows [17]:

$$i_{\mathrm{DG_{ref}}} = \underbrace{\frac{P_{\mathrm{DG}}k_1}{|v^{+}_{\mathrm{PCC}}|^2}v^{+}_{\mathrm{PCC}}}_{i^{+}_{\mathrm{DG_p}}} + \underbrace{\frac{P_{\mathrm{DG}}(1-k_1)}{|v^{-}_{\mathrm{PCC}}|^2}v^{-}_{\mathrm{PCC}}}_{i^{-}_{\mathrm{DG_p}}} + \underbrace{\frac{Q_{\mathrm{DG}}k_2}{|v^{+}_{\mathrm{PCC}}|^2}v^{+}_{\mathrm{PCC_\perp}}}_{i^{+}_{\mathrm{DG_q}}} + \underbrace{\frac{Q_{\mathrm{DG}}(1-k_2)}{|v^{-}_{\mathrm{PCC}}|^2}v^{-}_{\mathrm{PCC_\perp}}}_{i^{-}_{\mathrm{DG_q}}}. \quad (6)$$

Considering (6), the positive and negative sequences DG's reference current vectors can be expressed as follows:

$$i^{+}_{\mathrm{DG_{ref}}} = \underbrace{\left(\frac{P_{\mathrm{DG}}k_1}{|v^{+}_{\mathrm{PCC}}|^2} - \frac{Q_{\mathrm{DG}}k_2}{|v^{+}_{\mathrm{PCC}}|^2}e^{j\frac{\pi}{2}}\right)}_{Y^{+}_{\mathrm{DG}}} v^{+}_{\mathrm{PCC}} \quad (7)$$

$$i^{-}_{\mathrm{DG_{ref}}} = \underbrace{\left(\frac{P_{\mathrm{DG}}(1-k_1)}{|v^{-}_{\mathrm{PCC}}|^2} + \frac{Q_{\mathrm{DG}}(1-k_2)}{|v^{-}_{\mathrm{PCC}}|^2}e^{j\frac{\pi}{2}}\right)}_{Y^{-}_{\mathrm{DG}}} v^{-}_{\mathrm{PCC}}. \quad (8)$$

According to (7) and (8), the DG's positive and negative sequence virtual admittances can be controlled by weighting factors k_1 and k_2, leading to DG's output current (or in other words power) adjustment. From (3), (4), and (6), the active and reactive powers oscillations at the DG output can be achieved as follows:

$$\tilde{p}_{\mathrm{DG}} = \left(\frac{P_{\mathrm{DG}}k_1}{|v^{+}_{\mathrm{PCC}}|^2} + \frac{P_{\mathrm{DG}}(1-k_1)}{|v^{-}_{\mathrm{PCC}}|^2}\right) v^{+}_{\mathrm{PCC}} \cdot v^{-}_{\mathrm{PCC}} + \left(\frac{Q_{\mathrm{DG}}k_2}{|v^{+}_{\mathrm{PCC}}|^2} - \frac{Q_{\mathrm{DG}}(1-k_2)}{|v^{-}_{\mathrm{PCC}}|^2}\right) v^{+}_{\mathrm{PCC_\perp}} \cdot v^{-}_{\mathrm{PCC}} \quad (9)$$

$$\tilde{q}_{\mathrm{DG}} = \left(\frac{P_{\mathrm{DG}}k_1}{|v^{+}_{\mathrm{PCC}}|^2} - \frac{P_{\mathrm{DG}}(1-k_1)}{|v^{-}_{\mathrm{PCC}}|^2}\right) v^{+}_{\mathrm{PCC}} \cdot v^{-}_{\mathrm{PCC_\perp}} + \left(\frac{Q_{\mathrm{DG}}k_2}{|v^{+}_{\mathrm{PCC}}|^2} + \frac{Q_{\mathrm{DG}}(1-k_2)}{|v^{-}_{\mathrm{PCC}}|^2}\right) v^{+}_{\mathrm{PCC_\perp}} \cdot v^{-}_{\mathrm{PCC_\perp}}. \quad (10)$$

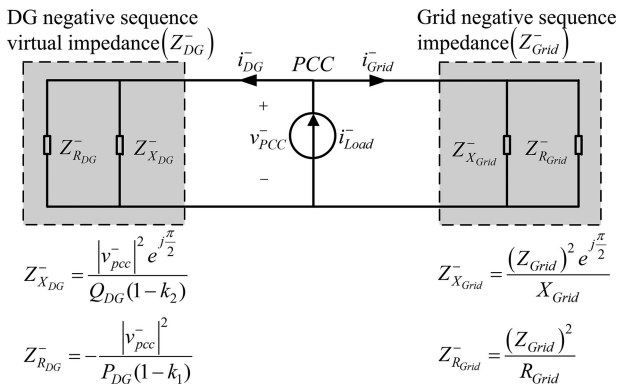

Fig. 2. Negative sequence model of the grid-connected DG.

III. Sequence Network Model of Grid-Connected DG

The three-phase unbalanced power system can be represented by positive, negative, and zero sequence components and their equivalent sequence networks. Depending on the configuration of unbalance load connected to the three-phase power system, these equivalent sequence networks are connected to each other in different configurations [24]. Fig. 2 shows the equivalent negative sequence model of the grid-connected DG (no zero sequence in the system). In this figure, the positive sequence equivalent network together with unbalance load is represented by an equivalent current source i^{-}_{load} (whose value depends on the unbalance load configuration as well as the positive sequence network parameters as will be discussed later). Moreover, in Fig. 2, DG is represented as a virtual impedance Z^{-}_{DG} in order to emulate its behavior in the negative sequence circuit (see (8)), the grid negative sequence impedance (Z^{-}_{Grid}) is shown in parallel configuration, and the currents directions are assumed as shown in figure for better explanation.

If the three-phase unbalance load is connected to the PCC in star connection (Z_{L1}, Z_{L2}, Z_{L3}), i^{-}_{load} can be represented as (11) (Note that using three-phase network symmetrical component analysis, i^{-}_{load} can be extended to other load types, e.g., single-phase load) eqn. (11) as shown at the bottom of the page.

In (11), Z_L is the summation of load impedances ($Z_L = Z_{L1} + Z_{L2} + Z_{L3}$), and a is the rotation operator ($a = e^{j\frac{2\pi}{3}}$). Moreover, E represents the voltage of the PCC under balance condition (without presence of unbalance load), and Z^{+} and Z^{-} are positive and negative sequence impedances seen from the PCC. Considering Figs. 1 and 2, these parameters can be achieved as follows:

$$E = \frac{Z^{+}_{\mathrm{DG}}}{Z^{+}_{\mathrm{DG}} + Z^{+}_{\mathrm{Grid}}} \times v_g \quad (12)$$

$$Z^{+} = Z^{+}_{\mathrm{DG}} || Z^{+}_{\mathrm{Grid}} \quad (13)$$

$$Z^{-} = Z^{-}_{\mathrm{DG}} || Z^{-}_{\mathrm{Grid}} \quad (14)$$

$$i^{-}_{\mathrm{load}} = \frac{E\left(a^2 Z_{L1} + aZ_{L2} + Z_{L3}\right)}{Z_{L1}Z_{L3} + Z_{L2}Z_{L3} + Z_{L1}Z_{L2} + Z^{-}Z_L + Z^{+}Z_L + 3Z^{+}Z^{-}} \quad (11)$$

where Z^{+}_{Grid} is the grid positive sequence impedance, v_g is the grid voltage, and Z^{+}_{DG} is the DG's positive sequence virtual impedance that can be expressed as (15) using (7)

$$Z^{+}_{\mathrm{DG}} = Z^{+}_{R_{\mathrm{DG}}} || Z^{+}_{X_{\mathrm{DG}}} = \left(-\frac{\left|v^{+}_{\mathrm{PCC}}\right|^2}{P_{\mathrm{DG}} k_1} \right) || \left(\frac{\left|v^{+}_{\mathrm{PCC}}\right|^2}{Q_{\mathrm{DG}} k_2} e^{-j\frac{\pi}{2}} \right). \tag{15}$$

In the two proposed control strategies to be discussed later, for better explanation and comparison, i^{-}_{load} will be considered as a constant value based on the fixed values of $|i^{-}_{\mathrm{DG}}|$ and DG's active–reactive powers. Considering (11)–(15), this assumption is valid since Z^{+} and E are approximately constant values in the aforementioned conditions. Moreover, the variations of Z^{-} in the two proposed control strategies will not influence the denominator of (11) due to its small amplitude (in both the proposed control strategies, Z^{-}_{DG} is controlled to be much smaller than the grid impedance). However, it is worth mentioning again that this assumption is just for better explanations and comparison, and the proposed strategies are still valid without this assumption.

Considering the sequence network equivalent circuit in Fig. 2, two scenarios are discussed.

DG Produces Balance Current Without Unbalanced Voltage Compensation

In the case that weighting factors k_1 and k_2 are equal to 1 ($k_1 = 1$ and $k_2 = 1$), just positive sequence active and reactive powers are injected to the grid. From Fig. 2, both $Z^{-}_{R_{\mathrm{DG}}}$ and $Z^{-}_{X_{\mathrm{DG}}}$ are open circuit, and the negative sequence voltage of the PCC can be expressed as

$$\left|v^{-}_{\mathrm{PCC}}\right| = \left|i^{-}_{\mathrm{load}}\right| \times \left|Z^{-}_{\mathrm{Grid}}\right|. \tag{16}$$

DG Produces Unbalance Current for Unbalanced Voltage Compensation

In the case that weighting factors k_1 and k_2 are not equal to 1 ($k_1 \neq 1$ and $k_2 \neq 1$), positive and negative sequence active and reactive powers are injected to the grid. From Fig. 2, the negative sequence voltage of the PCC can be achieved as

$$\left|v^{-}_{\mathrm{PCC}}\right| = \left|i^{-}_{\mathrm{load}}\right| \times \left|Z^{-}_{\mathrm{Grid}} // Z^{-}_{\mathrm{DG}}\right|. \tag{17}$$

From (16), (17), and Fig. 2, it can be seen that injecting the negative sequence active and reactive powers to the grid by DG could compensate the PCC unbalanced voltage. In other words, the negative sequence virtual impedance of DG (Z^{-}_{DG}) can be controlled to be much smaller than the grid impedance, directing i^{-}_{load} to flow to the DG side and leading to an improved PCC voltage. However, how the control of DG negative sequence virtual impedance or negative sequence current can minimize the DG's output active power oscillation and effectively reduce the negative sequence voltage of PCC will be discussed in the following section.

IV. Two Proposed Control Strategies for Unbalanced Voltage Compensation

A. Unbalanced Voltage Compensation With Active Power Oscillation Minimization

As shown in (9), to compensate the PCC voltage unbalance, the DG negative sequence currents produce active power oscillation at the DG output, which leads to the dc-link voltage oscillation. The dc-link ripples have adverse effects on the dc-side power system (especially in hybrid ac/dc grid) and may produce harmonics at DGs ac output. In the active power oscillation cancellation strategy [12], the level of unbalanced voltage compensation cannot be controlled directly. Therefore, in order to control and compensate the grid steady-state unbalanced voltage and to reduce the adverse effects of this unbalance compensation, this proposed control strategy aims at minimizing the active power oscillation while with adjustable unbalance compensation levels. This strategy is named as the active power oscillation minimization or $\tilde{p}$-minimization strategy.

In this control strategy, the amplitude and phase angle of DG's negative sequence current is controlled (i.e., DG's negative sequence virtual impedance can be controlled which is the same approach) to minimize the active power oscillation and compensate unbalanced voltage. From (8), the amplitude of DG's desired negative sequence current is defined as follows:

$$\begin{aligned}\left|i^{-}_{\mathrm{DG_{ref}}}\right| &= \frac{\left|v^{-}_{\mathrm{PCC}}\right|}{\left|Z^{-}_{\mathrm{DG}}\right|} \\ &= \sqrt{\left(\frac{P_{\mathrm{DG}}(1-k_1)}{\left|v^{-}_{\mathrm{PCC}}\right|}\right)^2 + \left(\frac{Q_{\mathrm{DG}}(1-k_2)}{\left|v^{-}_{\mathrm{PCC}}\right|}\right)^2}.\end{aligned} \tag{18}$$

Based on (18), k_1 and k_2 are in the following boundary:

$$1 - \frac{\left|v^{-}_{\mathrm{PCC}}\right|\left|i^{-}_{\mathrm{DG_{ref}}}\right|}{P_{\mathrm{DG}}} \leqslant k_1 \leqslant 1 + \frac{\left|v^{-}_{\mathrm{PCC}}\right|\left|i^{-}_{\mathrm{DG_{ref}}}\right|}{P_{\mathrm{DG}}} \tag{19}$$

$$1 - \frac{\left|v^{-}_{\mathrm{PCC}}\right|\left|i^{-}_{\mathrm{DG_{ref}}}\right|}{Q_{\mathrm{DG}}} \leqslant k_2 \leqslant 1 + \frac{\left|v^{-}_{\mathrm{PCC}}\right|\left|i^{-}_{\mathrm{DG_{ref}}}\right|}{Q_{\mathrm{DG}}}. \tag{20}$$

In addition, considering (9), the active power oscillation in stationary $\alpha\beta$ reference frame can be achieved as follows:

$$\begin{aligned}\tilde{p}_{\mathrm{DG}} = {} & \frac{3}{2}\left(\frac{P_{\mathrm{DG}}k_1}{\left|v^{+}_{\mathrm{PCC}}\right|^2} + \frac{P_{\mathrm{DG}}(1-k_1)}{\left|v^{-}_{\mathrm{PCC}}\right|^2}\right) \\ & \times (v^{+}_{\mathrm{PCC}_\alpha} v^{-}_{\mathrm{PCC}_\alpha} + v^{+}_{\mathrm{PCC}_\beta} v^{-}_{\mathrm{PCC}_\beta}) \\ & + \frac{3}{2}\left(\frac{Q_{\mathrm{DG}}k_2}{\left|v^{+}_{\mathrm{PCC}}\right|^2} - \frac{Q_{\mathrm{DG}}(1-k_2)}{\left|v^{-}_{\mathrm{PCC}}\right|^2}\right) \\ & \times (v^{+}_{\mathrm{PCC}_\beta} v^{-}_{\mathrm{PCC}_\alpha} - v^{+}_{\mathrm{PCC}_\alpha} v^{-}_{\mathrm{PCC}_\beta}).\end{aligned} \tag{21}$$

Using Clarke transformation, the PCC positive and negative sequences voltage in stationary $\alpha\beta$ reference frame can be expressed as follows:

$$v^{+}_{\mathrm{PCC}_\alpha} = \left|v^{+}_{\mathrm{PCC}}\right| \cos\left(\omega t + \theta^{+}\right) \tag{22}$$

$$v^{+}_{\mathrm{PCC}_\beta} = \left|v^{+}_{\mathrm{PCC}}\right| \cos\left(\omega t - \frac{\pi}{2} + \theta^{+}\right) \tag{23}$$

$$v^{-}_{\mathrm{PCC}_\alpha} = \left|v^{-}_{\mathrm{PCC}}\right| \cos\left(\omega t - \theta^{-}\right) \tag{24}$$

$$v^{-}_{\mathrm{PCC}_\beta} = \left|v^{-}_{\mathrm{PCC}}\right| \cos\left(\omega t + \frac{\pi}{2} - \theta^{-}\right) \tag{25}$$

where θ^+ and θ^- are the phase angle jumps. From (21) to (25), the active power oscillation can be expressed as follows:

$$\begin{aligned}\tilde{p}_{\mathrm{DG}} = & \frac{3}{2}\left(\frac{P_{\mathrm{DG}}k_1}{\left|v_{\mathrm{PCC}}^+\right|^2}+\frac{P_{\mathrm{DG}}(1-k_1)}{\left|v_{\mathrm{PCC}}^-\right|^2}\right)\\ &\times\left|v_{\mathrm{PCC}}^+\right|\left|v_{\mathrm{PCC}}^-\right|\cos\left(2\omega t+\theta\right)\\ &+\frac{3}{2}\left(\frac{Q_{\mathrm{DG}}k_2}{\left|v_{\mathrm{PCC}}^+\right|^2}-\frac{Q_{\mathrm{DG}}(1-k_2)}{\left|v_{\mathrm{PCC}}^-\right|^2}\right)\\ &\times\left|v_{\mathrm{PCC}}^+\right|\left|v_{\mathrm{PCC}}^-\right|\sin\left(2\omega t+\theta\right)\end{aligned}\tag{26}$$

where $\theta^+-\theta^-=\theta$ is the phase angle between positive and negative sequences. In order to minimize sinusoidal active power oscillation in (26), following objective function is defined:

$$\begin{aligned}&\left[\left(\frac{P_{\mathrm{DG}}k_1}{\left|v_{\mathrm{PCC}}^+\right|^2}+\frac{P_{\mathrm{DG}}(1-k_1)}{\left|v_{\mathrm{PCC}}^-\right|^2}\right)\left|v_{\mathrm{PCC}}^+\right|\left|v_{\mathrm{PCC}}^-\right|\right]^2\\ &+\left[\left(\frac{Q_{\mathrm{DG}}k_2}{\left|v_{\mathrm{PCC}}^+\right|^2}-\frac{Q_{\mathrm{DG}}(1-k_2)}{\left|v_{\mathrm{PCC}}^-\right|^2}\right)\left|v_{\mathrm{PCC}}^+\right|\left|v_{\mathrm{PCC}}^-\right|\right]^2.\end{aligned}\tag{27}$$

This objective function should be minimized subjected to the constraint in (18) which provides controllable unbalanced voltage compensation. With the assumption of $k_1-1=l_1$ and $k_2-1=l_2$, the objective function in (27) and the constraint in (18) could be expressed

$$J\left(l_1,l_2\right)=A^2l_1^2+B^2l_2^2+Cl_1+El_2+F\tag{28}$$

$$P_{\mathrm{DG}}^2l_1^2+Q_{\mathrm{DG}}^2l_2^2=D^2\tag{29}$$

where $A,\ B,\ C,\ D,\ E$, and F are defined as

$$A=\frac{P_{\mathrm{DG}}\left(\left|v_{\mathrm{PCC}}^+\right|^2-\left|v_{\mathrm{PCC}}^-\right|^2\right)}{\left|v_{\mathrm{PCC}}^+\right|\left|v_{\mathrm{PCC}}^-\right|},$$

$$B=\frac{Q_{\mathrm{DG}}\left(\left|v_{\mathrm{PCC}}^+\right|^2+\left|v_{\mathrm{PCC}}^-\right|^2\right)}{\left|v_{\mathrm{PCC}}^+\right|\left|v_{\mathrm{PCC}}^-\right|},$$

$$C=\frac{2P_{\mathrm{DG}}^2\left|v_{\mathrm{PCC}}^-\right|^2\left(\left|v_{\mathrm{PCC}}^+\right|^2-\left|v_{\mathrm{PCC}}^-\right|^2\right)}{\left|v_{\mathrm{PCC}}^+\right|^2\left|v_{\mathrm{PCC}}^-\right|^2},$$

$$D=\left|v_{\mathrm{PCC}}^-\right|\left|i_{\mathrm{DG_{ref}}}^-\right|,$$

$$E=\frac{-2Q_{\mathrm{DG}}^2\left|v_{\mathrm{PCC}}^-\right|^2\left(\left|v_{\mathrm{PCC}}^+\right|^2+\left|v_{\mathrm{PCC}}^-\right|^2\right)}{\left|v_{\mathrm{PCC}}^+\right|^2\left|v_{\mathrm{PCC}}^-\right|^2},$$

$$\text{and}\quad F=\frac{\left|v_{\mathrm{PCC}}^-\right|^2\left(P_{\mathrm{DG}}^2+Q_{\mathrm{DG}}^2\right)}{\left|v_{\mathrm{PCC}}^+\right|^2\left|v_{\mathrm{PCC}}^-\right|^2}.$$

Considering (28) and (29), the closed-form analytical solution can be found using Lagrangian method [25]. Utilizing this deterministic method, l_1 and l_2 can be determined analytically as a function of the system operating point. Due to the limited computation and deterministic solution in comparison to heuristic optimization methods, these parameters can be easily updated online in a digital controller. From (28) and (29), the Lagrangian function is defined as follows:

$$\begin{aligned}L\left(l_1,l_2,\lambda\right) = & A^2l_1^2+B^2l_2^2+Cl_1+El_2+F\\ &+\lambda\left(P_{\mathrm{DG}}^2l_1^2+Q_{\mathrm{DG}}^2l_2^2-D^2\right)\end{aligned}\tag{30}$$

where λ is a Lagrangian multiplier. Setting each of the partial derivatives of this function equal to zero ($\frac{\partial L}{\partial l_1}=0$, $\frac{\partial L}{\partial l_2}=0$, $\frac{\partial L}{\partial \lambda}=0$), the optimal values of l_1 and l_2 are calculated analytically, leading to k_1 and k_2 determination. In control system, in each time step, l_1 and l_2 are updated based on system parameters.

B. Unbalanced Voltage Compensation With Inphase Current Compensation

In order to effectively compensate the grid unbalanced voltage, or in other words to minimize the PCC negative sequence voltage under a given DG's negative sequence current level, the phase angles of DG and the grid negative sequence currents should be the same. In this case, by assuming constant negative sequence load current (i_{load}^-) in the fixed $\left|i_{\mathrm{DG}}^-\right|$, minimum negative sequence current will be directed to the grid, resulting in a minimum negative sequence voltage at the PCC ($\left|v_{\mathrm{PCC}}^-\right|=\left|i_{\mathrm{Grid}}^-\right|\times\left|Z_{\mathrm{Grid}}^-\right|$). In this control strategy, the active power oscillation at the DG output is not controlled directly. In this paper, this strategy is named as inphase current compensation strategy.

In this control strategy, the amplitude and phase angle of DG's negative sequence current (or DG's negative sequence virtual impedance) is controlled to minimize the negative sequence voltage of the PCC without active power oscillation consideration. In this method, the phase angles of DG and the grid negative sequence impedances (see Fig. 2) are controlled to be the same as in

$$\measuredangle Z_{\mathrm{DG}}^-=\measuredangle Z_{\mathrm{Grid}}^-.\tag{31}$$

Considering (18) and (31), k_1 and k_2 can be achieved as follows:

$$k_1 = 1\pm\frac{\left|v_{\mathrm{PCC}}^-\right|\left|i_{\mathrm{DG_{ref}}}^-\right|}{P_{\mathrm{DG}}\times\sqrt{1+\left(\frac{Z_{X_{\mathrm{Grid}}}^-}{Z_{R_{\mathrm{Grid}}}^-}\right)^2}}\tag{32}$$

$$k_2 = 1\pm\frac{Z_{X_{\mathrm{Grid}}}^-}{Z_{R_{\mathrm{Grid}}}^-}\times\frac{\left|v_{\mathrm{PCC}}^-\right|\left|i_{\mathrm{DG_{ref}}}^-\right|}{Q_{\mathrm{DG}}\times\sqrt{1+\left(\frac{Z_{X_{\mathrm{Grid}}}^-}{Z_{R_{\mathrm{Grid}}}^-}\right)^2}}.\tag{33}$$

Considering (18), (32), and (33), it can be concluded that if $k_1>1$ and $k_2<1$, DG's negative sequence current will be inphase with the grid negative sequence current. However, $k_1<1$ and $k_2>1$ will cause them to be 180° out of phase. Considering (32) and (33), in this strategy just the ratio of the grid reactance to resistance in fundamental frequency is needed, which can be easily obtained using different methods [26]–[28]. In this paper, this ratio is considered as a known value in the control system.

Finally, the overall control block diagram is shown in Fig. 3. This control system contains an outer loop which is responsible

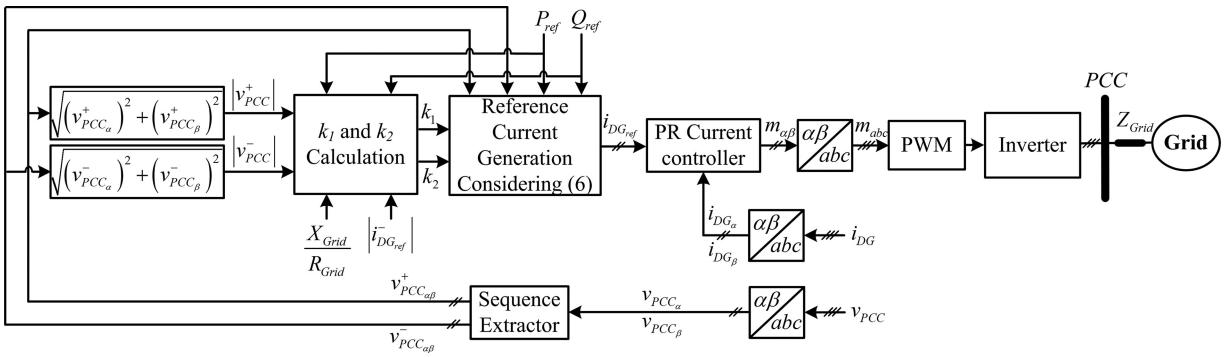

Fig. 3. Proposed control strategies of DG for the grid unbalanced voltage compensation.

TABLE I
CASE STUDY RESULTS FOR BOTH PROPOSED CONTROL STRATEGIES WITH $|i^-_{\mathrm{DG_{ref}}}| = 10$ A UNDER DIFFERENT DG'S OUTPUT P/Q RATIOS ($S_{\mathrm{DG}} = 20.61$ KVA) AND THE GRID CONDITIONS ($|Z_{\mathrm{Grid}}| = 0.75398\ \Omega$)

	Grid impedance conditions	$X_{\mathrm{Grid}} \gg R_{\mathrm{Grid}}$ $R = 0.001\ \Omega$ $X = 0.753\ \Omega$		$X_{\mathrm{Grid}} \ll R_{\mathrm{Grid}}$ $R = 0.753\ \Omega$ $X = 0.001\ \Omega$	
	DG's output active–reactive powers	20 kW 5 kVar	5 kW 20 kVar	20 kW 5 kVar	5 kW 20 kVar
$\lvert v^-_{\mathrm{PCC}}\rvert$	No compensation	13.66	15.70	12.88	10.74
	$\tilde{p}$-minimization	9.10	8.26	6.25	6.88
	Inphase current	6.23	8.26	6.15	4.00
	$\frac{\tilde{p}-\mathrm{minimization}}{\mathrm{In\text{-}phase\ current}}$ ratio	1.46	1	1.01	1.72
$\tilde{p}$	No compensation	1368	1368	1228	1228
	$\tilde{p}$-minimization	2177	2835	2643	1921
	Inphase current	3005	2862	2673	2626
	$\frac{\tilde{p}-\mathrm{minimization}}{\mathrm{In\text{-}phase\ current}}$ ratio	0.72	0.99	0.98	0.73
$\tilde{q}$	No compensation	1368	1368	1228	1228
	$\tilde{p}$-minimization	4007	4267	3840	3487
	Inphase current	3297	4248	3820	2850
	$\frac{\tilde{p}-\mathrm{minimization}}{\mathrm{In\text{-}phase\ current}}$ ratio	1.21	1.004	1.005	1.22

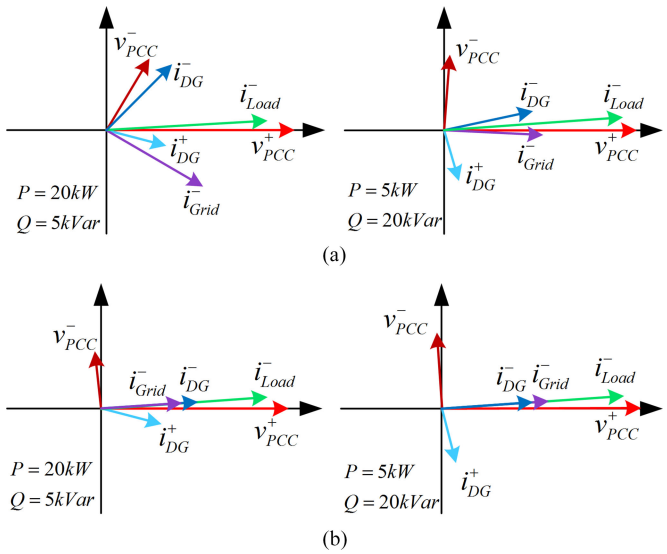

Fig. 4. Phasor diagrams of the case study in phase-a with $|i^-_{\mathrm{DG_{ref}}}| = 10$ A under $X_{\mathrm{Grid}} \gg R_{\mathrm{Grid}}$ and different P/Q ratios at DG output (v^+_{PCC} and i^+_{DG} with the scale of 0.1); (a) $\tilde{p}$-minimization, (b) inphase current compensation strategy.

for DG's reference current generation, and an inner current control loop which is responsible for tracking the reference current quickly and accurately. The control is implemented in the stationary $\alpha\beta$ reference frame to avoid multiple frame transformations for different sequence components control. In the outer loop, among different sequence extractors [29]–[31], frequency-locked loop-based sequence extractor in [31] is used to separate the PCC voltage into positive and negative sequences. Moreover, weighting factors k_1 and k_2 are determined by either the active power oscillation minimization or inphase current compensation strategy. In Fig. 3, $|i^-_{\mathrm{DG_{ref}}}|$ can be set directly through the desired DG's negative sequence virtual impedance using (18). Either way, the DG's available rating for unbalance compensation need to be a constraint. In the inner control loop, DG's interfacing converter is controlled in the current control operation mode using proportional-resonant controller [32].

V. COMPARISONS OF THE PROPOSED STRATEGIES

In this section, detailed study of each proposed control strategy and their differences are concluded, and the influences of DG's operating conditions in terms of output P/Q ratios and the grid conditions in terms of different $X_{\mathrm{Grid}}/R_{\mathrm{Grid}}$ ratios are investigated. These discussions are supported by a case study in Table I and Figs. 4 and 5, where a three-phase grid interfacing DG system is simulated. In this case study, for better explanation and comparison, the performance of the two proposed control strategies in normal grid with inductive impedance (large $X_{\mathrm{Grid}}/R_{\mathrm{Grid}}$ ratio) and weak grid with resistive impedance (small $X_{\mathrm{Grid}}/R_{\mathrm{Grid}}$ ratio) under different DG's output P/Q ratio are presented. The DG's apparent power (S_{DG}) and the amplitude of the grid impedance ($|Z_{\mathrm{Grid}}|$) are considered to be constant. Complete simulation results and the parameters and specifications of the simulated system will be provided in Section VI.

First of all, with DG's compensation and the equivalent small negative sequence virtual impedance, the negative sequence load current is directed to the DG side, resulting in less negative sequence current in the grid (i^-_{Grid}) and, therefore, the negative sequence voltage at the PCC are reduced in all conditions in both the proposed methods. However, considering (3) and (4),

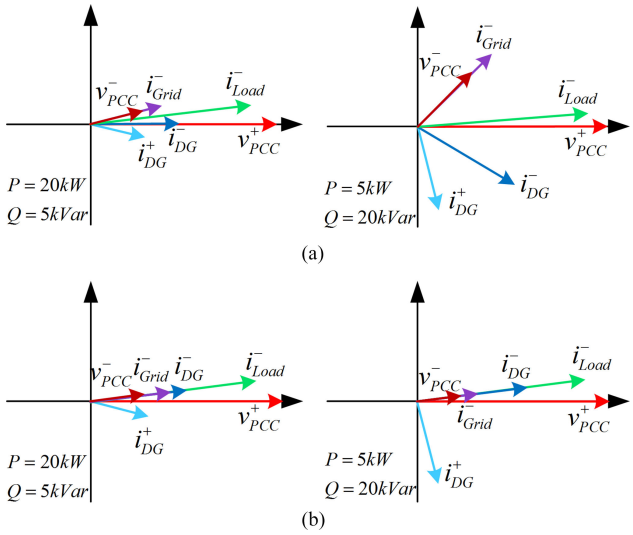

Fig. 5. Phasor diagrams of the case study in phase-a with $|i^-_{\mathrm{DG_{ref}}}| = 10$ A under $X_{\mathrm{Grid}} \ll R_{\mathrm{Grid}}$ and different P/Q ratios at DG output (v^+_{PCC} and i^+_{DG} with the scale of 0.1); (a) $\tilde{p}$-minimization, (b) inphase current compensation strategy.

TABLE II
SYSTEM PARAMETERS FOR SIMULATIONS

	Symbol	Value
DC-link voltage	v_{dc}	800 V
DG's reference active power	P_{ref}	20 kW → 5 kW
DG's reference reactive power	Q_{ref}	5 kVar → 20 kVar
Three phase unbalance load	R_{Load}	Three phase: 18, 5, 3 Ω
Grid phase voltage (rms)	v_g	240 V
Grid frequency	f_g	60 Hz
Grid coupling impedance	Z_{Grid}	X_{Grid} : 0.753 Ω → 1 mΩ R_{Grid} : 1 mΩ → 0.753 Ω

the presence of i^-_{DG} increase the active and reactive powers oscillations in comparison to balance current injection. These results can be confirmed by Table I.

In the active power oscillation minimization strategy, DG's negative sequence current (or DG's negative sequence virtual impedance) is controlled in order to minimize the active power oscillation at DG output. Therefore, the active power oscillation in this strategy is smaller than the inphase current compensation method in all operating conditions ($\tilde{p}_{\tilde{p}-\mathrm{minimization}} < \tilde{p}_{\mathrm{inphase}}$). As shown in Table I, the ratios of active power oscillation in $\tilde{p}$-minimization strategy over inphase current compensation strategy are always less than 1 under the same operating conditions. At the same time, it can also be observed that the reactive power oscillations in the active power oscillation minimization will be larger than inphase current compensation ($\tilde{q}_{\tilde{p}-\mathrm{minimization}} > \tilde{q}_{\mathrm{inphase}}$). This is because, considering (9) and (27), for active power oscillation minimization $|P(1-k_1)/|v^-_{\mathrm{PCC}}|^2|$ and $|Q(1-k_2)/|v^-_{\mathrm{PCC}}|^2|$ should reach $-|Pk_1/|v^+_{\mathrm{PCC}}|^2|$ and $|Qk_2/|v^+_{\mathrm{PCC}}|^2|$, respectively. In this case, the reactive power oscillations will increase according to (10).

For the inphase current compensation strategy, the phase angles of i^-_{load}, i^-_{DG}, and i^-_{Grid} are the same. Obviously, with the same $|i^-_{\mathrm{load}}|$ and $|i^-_{\mathrm{DG}}|$, i^-_{Grid} in the inphase current compensation strategy will be smaller than the $\tilde{p}$-minimization strategy ($|i^-_{\mathrm{Grid}}|_{\tilde{p}-\mathrm{minimization}} > |i^-_{\mathrm{Grid}}|_{\mathrm{inphase}}$). The relationship is more clearly shown in the phasor plot in Figs. 4 and 5. Therefore, the negative sequence voltage at the PCC in the inphase current compensation will be smaller than the active power oscillation minimization strategy ($|v^-_{\mathrm{PCC}}|_{\tilde{p}-\mathrm{minimization}} > |v^-_{\mathrm{PCC}}|_{\mathrm{inphase}}$). As shown in Table I, the ratios of negative sequence voltage in the $\tilde{p}$-minimization strategy over inphase current compensation are always greater than 1 under the same operating conditions.

In both the methods, increasing $|i^-_{\mathrm{DG}}|$ will reduce $|i^-_{\mathrm{Grid}}|$, which leads to more reduction of negative sequence voltage at PCC. However, considering (3) and (4), the active and reactive powers oscillation will increase with higher unbalance compensation level. In small DGs, due to lower $|i^-_{\mathrm{DG}}|$, performance difference of the two proposed control strategies in terms of the negative sequence voltage reduction will not be very obvious. Therefore, the active power oscillation will be a dominant factor when comparing the two methods. On the other hand, in large DGs, due to possibility of high $|i^-_{\mathrm{DG}}|$, the difference negative sequence voltage reduction between the two methods will be more obvious and become a dominant factor when comparing the two methods. The influence of $|i^-_{\mathrm{DG}}|$ in the two proposed methods will be shown in the Section VI. Additional comparisons of the two proposed strategies are provided in the following sections.

A. Inductive Grid Under Various DG's Output P/Q Ratios

The performance of the two proposed methods in normal grid with inductive impedance where X_{Grid} is much large than R_{Grid} ($X_{\mathrm{Grid}} \gg R_{\mathrm{Grid}}$) is studied. In the inductive grid impedance, the negative sequence current of the grid and the negative sequence voltage of PCC are approximately orthogonal.

In the $\tilde{p}$-minimization strategy, with small values of P/Q ratio ($P \ll Q$) at the DG output when DG mainly produces reactive power support, the phase angle between v^-_{PCC} and i^-_{DG} will be close to 90° according to (8). As a result, the DG and the grid negative sequence currents will be approximately inphase (small phase angle between i^-_{DG} and i^-_{Grid}). This can also be seen in phasor plots in Figs. 4 and 5. Therefore, with inductive grid impedance, the results of active power oscillation minimization and inphase current compensation strategies are approximately the same in small P/Q ratios at the DG output. As shown in Table I, the ratios of negative sequence voltage and active and reactive power oscillations in $\tilde{p}$-minimization strategy over inphase current compensation are 1, 0.99, and 1.004, respectively. On the other hand, if DG operates with unity or high power factor, the performance difference of the two methods will be very obvious in terms of active power oscillation and effectiveness of negative sequence voltage reduction (see Table I, in which the negative sequence voltage of $\tilde{p}$-minimization strategy is 1.46 times larger than inphase current compensation, while its active power oscillation is 0.72 of inphase current compensation).

Moreover, in both the methods, the ratio of P/Q at the DG output will influence the effectiveness of $|v^-_{\mathrm{PCC}}|$ reduction. For the active power oscillation minimization, this is straightforward to understand as lower P/Q ratio makes this method performance closer to the inphase current compensation (see Figs. 4

TABLE III
SIMULATION RESULTS FOR TWO PROPOSED CONTROL STRATEGIES WITH $|i^-_{\mathrm{DG}_{\mathrm{ref}}}| = 5$ A UNDER DIFFERENT DG'S OUTPUT P/Q RATIOS AND THE GRID CONDITIONS

Grid impedance conditions		$X_{\mathrm{Grid}} \gg R_{\mathrm{Grid}}$ $R = 1\times10^{-3}\ \Omega;\ X = 0.753\ \Omega$			$X_{\mathrm{Grid}} = R_{\mathrm{Grid}}$ $R = 0.533\ \Omega;\ X = 0.533\ \Omega$			$X_{\mathrm{Grid}} \ll R_{\mathrm{Grid}}$ $R = 0.753\ \Omega;\ X = 1\times10^{-3}\ \Omega$		
DG's output active-reactive powers		20 kW 5 kVar	14.5 kW 14.5 kVar	5 kW 20 kVar	20 kW 5 kVar	14.5 kW 14.5 kVar	5 kW 20 kVar	20 kW 5 kVar	14.5 kW 14.5 kVar	5 kW 20 kVar
$\lvert i^-_{Grid}\rvert$	No compensation	18.12	20.00	20.82	17.70	18.10	17.40	17.08	16.13	14.24
	$\tilde{p}$-minimization	15.75	15.87	15.90	13.50	13.51	13.46	12.74	12.66	12.48
	Inphase current	13.20	15.10	15.90	13.14	13.51	12.85	12.60	11.70	9.80
$\lvert i^-_{Load}\rvert$	No compensation	18.12	20.00	20.82	17.74	18.15	17.45	17.08	16.13	14.24
	$\tilde{p}$-minimization	17.68	19.78	20.85	17.79	18.51	17.94	17.60	16.60	14.50
	Inphase current	18.20	20.10	20.90	18.14	18.51	17.85	17.60	16.70	14.80
$\lvert v^-_{PCC}\rvert$	No compensation	13.66	15.08	15.70	13.35	13.64	13.13	12.88	12.16	10.74
	$\tilde{p}$-minimization	11.88	11.97	11.99	10.18	10.19	10.15	9.59	9.54	9.41
	Inphase current	10.00	11.36	11.97	9.90	10.18	9.68	9.50	8.70	7.40
$\tilde{p}$	No compensation	1368	1368	1368	1264	1264	1264	1228	1228	1228
	$\tilde{p}$-minimization	351	619	734	668	723	630	705	568	280
	Inphase current	1624	1220	805	960	723	937	770	1100	1405
$\tilde{q}$	No compensation	1368	1368	1368	1264	1264	1264	1228	1228	1228
	$\tilde{p}$-minimization	2738	2790	2815	2600	2613	2580	2540	2495	2425
	Inphase current	2028	2536	2795	2485	2613	2452	2516	2252	1762

and 5), leading to more effective $|v^-_{\mathrm{PCC}}|$ reduction as explained earlier (see Table I, $|v^-_{\mathrm{PCC}}|$ is 9.10 V with $P/Q = 4$ and 8.26 V with $P/Q = 1/4$).

For the inphase current compensation, increasing P/Q ratio will cause more reduction of $|v^-_{\mathrm{PCC}}|$ (8.26 V with $P/Q = 1/4$ to 6.23 V with $P/Q = 4$ as shown in Table I). The reason is that since i^-_{DG} is inphase with i^-_{Grid} (i^-_{Grid} and v^-_{PCC} are approximately orthogonal in the normal inductive grid), considering (8), the reactive power component of i^-_{DG} will be much larger than the active power component ($|\frac{Q(1-k_2)}{|v^-_{\mathrm{PCC}}|^2}| \gg |\frac{P(1-k_1)}{|v^-_{\mathrm{PCC}}|^2}|$) (see Figs. 4 and 5). In other words, k_1 is very close to 1. As a result, considering equivalent circuit in Fig. 2, $Z^-_{R_{DG}}$ can be considered as an open circuit. Therefore, $|i^-_{\mathrm{DG}}|$ can be achieved as $|i^-_{\mathrm{DG}}| = \frac{|v^-_{\mathrm{PCC}}|}{Z^-_{X_{\mathrm{DG}}}} = \frac{Q(1-k_2)}{|v^-_{\mathrm{PCC}}|}$. Considering $|i^-_{\mathrm{DG}}|$ as a fixed value, increasing the value of Q will lead to $|v^-_{\mathrm{PCC}}|$ enhancement.

B. Weak Grid Under Various DG's Output P/Q Ratios

In the weak grid, the ratio of $X_{\mathrm{Grid}}/R_{\mathrm{Grid}}$ is small, and the grid has higher resistance. Here, in order to better explain the difference of the two proposed methods, the grid impedance with small $X_{\mathrm{Grid}}/R_{\mathrm{Grid}}$ ratios ($X_{\mathrm{Grid}} \ll R_{\mathrm{Grid}}$) is studied. The conclusions can be extended to the weak grids with comparable X_{Grid} and R_{Grid}, which will be discussed in Section VI.

In the weak grid with small $X_{\mathrm{Grid}}/R_{\mathrm{Grid}}$ ratio, the phase angle between negative sequence grid current and the negative sequence PCC voltage is small. In the $\tilde{p}$-minimization strategy in large values of P/Q ratio ($P \gg Q$) at the DG output with high power factor, the phase angle between v^-_{PCC} and i^-_{DG} will be small according to (8). As a result, i^-_{DG} and i^-_{Grid} will be approximately inphase (small phase angle between i^-_{DG} and i^-_{Grid}). This can be seen in phasor plots in Figs. 4 and 5. Therefore, the results of the active power oscillation minimization strategy and inphase current compensation are approximately the same in large P/Q ratios at DG output. As shown in Table I, the ratios of negative sequence voltage and active and reactive powers oscillations in $\tilde{p}$-minimization strategy over inphase current compensation are 1.01, 0.98, and 1.005, respectively. So if high power factor control of the DG is required, the two methods will perform similarly under weak grid condition with small $X_{\mathrm{Grid}}/R_{\mathrm{Grid}}$ ratios.

Similarly, the value of P/Q ratio at DG output will affect the effectiveness of $|v^-_{\mathrm{PCC}}|$ reduction in both methods under a weak grid. As explained earlier, increasing P/Q ratio will make the $\tilde{p}$-minimization strategy performance closer to the inphase current compensation in a weak grid condition (see Figs. 4 and 5), and therefore, high P/Q ratio will be more effective for $|v^-_{\mathrm{PCC}}|$ reduction under the active power oscillation minimization method. As shown in Table I, $|v^-_{\mathrm{PCC}}|$ is changed from 6.88 V with $P/Q = 1/4$ to 6.25 V with $P/Q = 4$.

For the inphase current compensation, decreasing P/Q ratio at DG output will cause more reduction of $|v^-_{\mathrm{PCC}}|$ (6.15 V with $P/Q = 4$ to 4 V with $P/Q = 1/4$ as shown in Table I). The reason is that since i^-_{DG} is inphase with i^-_{Grid}, considering (8), the active power component of i^-_{DG} will be much larger than the reactive power component ($|\frac{Q(1-k_2)}{|v^-_{\mathrm{PCC}}|^2}| \ll |\frac{P(1-k_1)}{|v^-_{\mathrm{PCC}}|^2}|$) (see Figs. 4 and 5). In other words, k_2 is very close to 1. As a result, considering equivalent circuit in Fig. 2, $Z^-_{X_{\mathrm{DG}}}$ can be considered as an open circuit. Therefore, $|i^-_{\mathrm{DG}}|$ can be achieved as $|i^-_{\mathrm{DG}}| = \frac{|v^-_{\mathrm{PCC}}|}{Z^-_{\mathrm{RDG}}} = \frac{P(1-k_1)}{|v^-_{\mathrm{PCC}}|}$. Considering $|i^-_{\mathrm{DG}}|$ as a fixed value, increasing the value of P will lead to $|v^-_{\mathrm{PCC}}|$ enhancement.

Additional comparisons and discussions of the two methods are presented in Sections VI and VII.

TABLE IV
SIMULATION RESULTS FOR TWO PROPOSED CONTROL STRATEGIES WITH $|i^-_{\mathrm{DG}_{\mathrm{ref}}}| = 10$ A UNDER DIFFERENT DG'S OUTPUT P/Q RATIOS AND THE GRID CONDITIONS

Grid impedance conditions		$X_{\mathrm{Grid}} \gg R_{\mathrm{Grid}}$ $R = 1\times10^{-3}\ \Omega;\ X = 0.753\ \Omega$			$X_{\mathrm{Grid}} = R_{\mathrm{Grid}}$ $R = 0.533\ \Omega;\ X = 0.533\ \Omega$			$X_{\mathrm{Grid}} \ll R_{\mathrm{Grid}}$ $R = 0.753\ \Omega;\ X = 1\times10^{-3}\ \Omega$		
DG's output active–reactive powers		20 kW 5 kVar	14.5 kW 14.5 kVar	5 kW 20 kVar	20 kW 5 kVar	14.5 kW 14.5 kVar	5 kW 20 kVar	20 kW 5 kVar	14.5 kW 14.5 kVar	5 kW 20 kVar
$\lvert i^-_{\mathrm{Grid}}\rvert$	No compensation	18.12	20.00	20.82	17.70	18.10	17.40	17.08	16.13	14.24
	$\tilde{p}$-minimization	12.07	11.28	10.96	9.04	8.93	9.09	8.30	8.50	9.10
	Inphase current	8.26	10.13	10.96	8.56	8.93	8.26	8.20	7.20	5.30
$\lvert i^-_{\mathrm{Load}}\rvert$	No compensation	18.12	20.00	20.82	17.74	18.15	17.45	17.08	16.13	14.24
	$\tilde{p}$-minimization	17.42	19.63	20.80	18.35	18.93	18.41	18.17	17.14	15.12
	Inphase current	18.26	20.13	20.95	18.56	18.93	18.26	18.20	17.20	15.30
$\lvert v^-_{\mathrm{PCC}}\rvert$	No compensation	13.66	15.08	15.70	13.35	13.64	13.13	12.88	12.16	10.74
	$\tilde{p}$-minimization	9.10	8.50	8.26	6.82	6.73	6.85	6.25	6.41	6.88
	Inphase current	6.23	7.64	8.26	6.45	6.73	6.22	6.15	5.44	4.00
$\tilde{p}$	No compensation	1368	1368	1368	1264	1264	1264	1228	1228	1228
	$\tilde{p}$-minimization	2177	2640	2835	2620	2707	2550	2643	2413	1921
	Inphase current	3005	2965	2862	2760	2710	2715	2673	2697	2626
$\tilde{q}$	No compensation	1368	1368	1368	1264	1264	1264	1228	1228	1228
	$\tilde{p}$-minimization	4007	4183	4267	3917	3956	3866	3840	3710	3487
	Inphase current	3297	3927	4248	3803	3959	3738	3820	3473	2850

VI. SIMULATIONS AND EXPERIMENTS

In order to verify the effectiveness and performance of the two proposed control strategies, simulation and experimental results are provided.

A. Simulation Verification

A three-phase grid interfacing DG system has been simulated utilizing the two proposed control strategies in MATLAB/Simulink. The simulated system parameters are shown in Table II.

In these simulations, in order to investigate the performance of the two proposed methods under different grid conditions and DG operating conditions, and to study the influence of DG's size on the compensation strategies, the results for $|i^-_{\mathrm{DG}_{\mathrm{ref}}}| = 5\,\mathrm{A}$ and $|i^-_{\mathrm{DG}_{\mathrm{ref}}}| = 10\,\mathrm{A}$ under different DG's output P/Q ratios and the grid $X_{\mathrm{Grid}}/R_{\mathrm{Grid}}$ ratios are shown in Tables III and IV.

In all the simulations, DG's apparent power and the amplitude of grid impedance are considered to be constant $S_{\mathrm{DG}} = 20.61$ kVA and $|Z_{\mathrm{Grid}}| = 0.75398\ \Omega$. For better comparison, the results of balance current injection from DG without compensation ($k_1 = k_2 = 1$) are presented too.

Considering the results in Tables III and IV, the following conclusions can be achieved that verify the previous discussions in Sections IV and V.

1) The i^-_{load} is approximately constant in the fixed $|i^-_{\mathrm{DG}_{\mathrm{ref}}}|$ and DG's active–reactive powers. Negative sequence voltage at the PCC is reduced utilizing the two proposed control strategies in all DG's operating conditions and the grid $X_{\mathrm{Grid}}/R_{\mathrm{Grid}}$ ratios.
2) The PCC negative sequence voltage in the inphase current compensation is smaller than the active power oscillation minimization strategy.
3) The active power oscillation minimization provides the minimum active power oscillation in each operation point. However, reactive power oscillation in this method is larger than the inphase current compensation strategy.
4) In the inductive grid if DG works as a reactive power compensator ($P \ll Q$), or in the weak grid if DG works with high power factor ($P \gg Q$), performance of two proposed control strategies are similar and the results of these strategies are close to each other.
5) In the inductive grid if DG works with high power factor ($P \gg Q$), or in the weak grid if DG works as a reactive power compensator ($P \ll Q$), performance difference of the two methods will be very obvious in terms of active power oscillation and the effectiveness of negative sequence voltage reduction.
6) In both the proposed control strategies, increasing $|i^-_{\mathrm{DG}_{\mathrm{ref}}}|$ causes more reduction of $|i^-_{\mathrm{Grid}}|$, resulting in more reduction of $|v^-_{\mathrm{PCC}}|$. However, the active and reactive powers oscillations increase in both methods.
7) With higher $|i^-_{\mathrm{DG}_{\mathrm{ref}}}|$, difference of the two proposed strategies in terms of unbalanced voltage compensation is more obvious.

The waveforms of simulation results in the two proposed control strategies with $|i^-_{\mathrm{DG}_{\mathrm{ref}}}| = 10\,\mathrm{A}$ (see Table IV) for inductive grid (with $X_{\mathrm{Grid}} \gg R_{\mathrm{Grid}}$) and weak grid (with $X_{\mathrm{Grid}} \ll R_{\mathrm{Grid}}$) are shown in Figs. 6–8 and Figs. 9–11, respectively. In these simulations during $t < 0.1$, the DG produces balance current ($k_1 = k_2 = 1$). At $t = 0.1$, the proposed control strategies are applied to the grid-connected DG system. During $0.1 < t < 0.4$, the DG's output active and reactive powers are $P_{\mathrm{ref}} = 20$ kW, $Q_{\mathrm{ref}} = 5$ kVAR, while during $0.4 < t < 0.7$ and $0.7 < t < 1$, these powers are set on $P_{\mathrm{ref}} = 14.5$ kW, $Q_{\mathrm{ref}} = 14.5$ kVAR and $P_{\mathrm{ref}} = 5$ kW, $Q_{\mathrm{ref}} = 20$ kVAR, respectively.

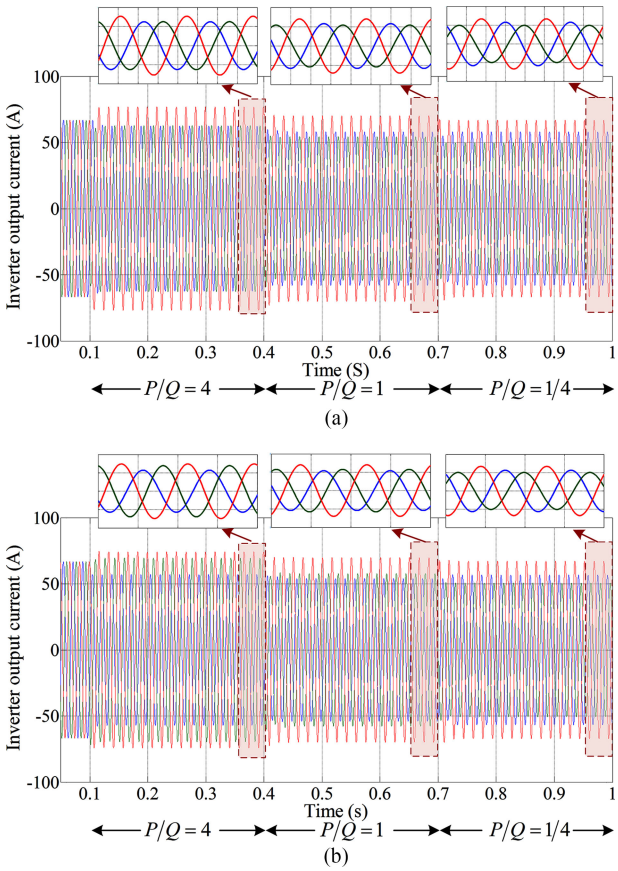

Fig. 6. Inverter output current in the inductive grid; (a) $\tilde{p}$-minimization strategy, (b) inphase current compensation.

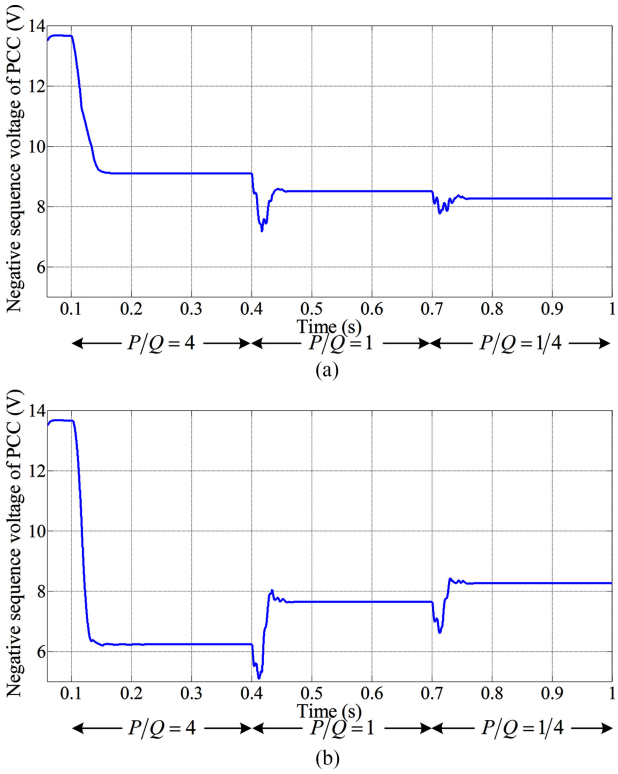

Fig. 7. Negative sequence voltage of PCC in the inductive grid; (a) $\tilde{p}$-minimization, (b) inphase current compensation.

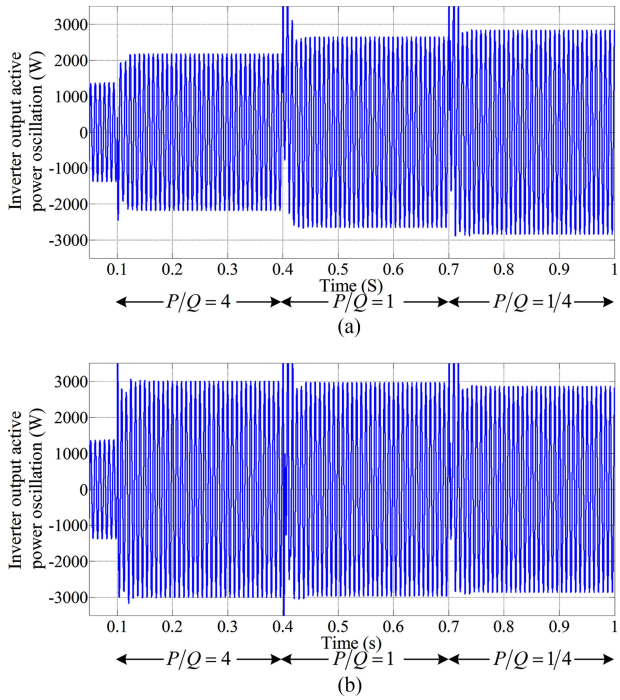

Fig. 8. Active power oscillations at the DG output in the inductive grid; (a) $\tilde{p}$-minimization, (b) inphase current compensation.

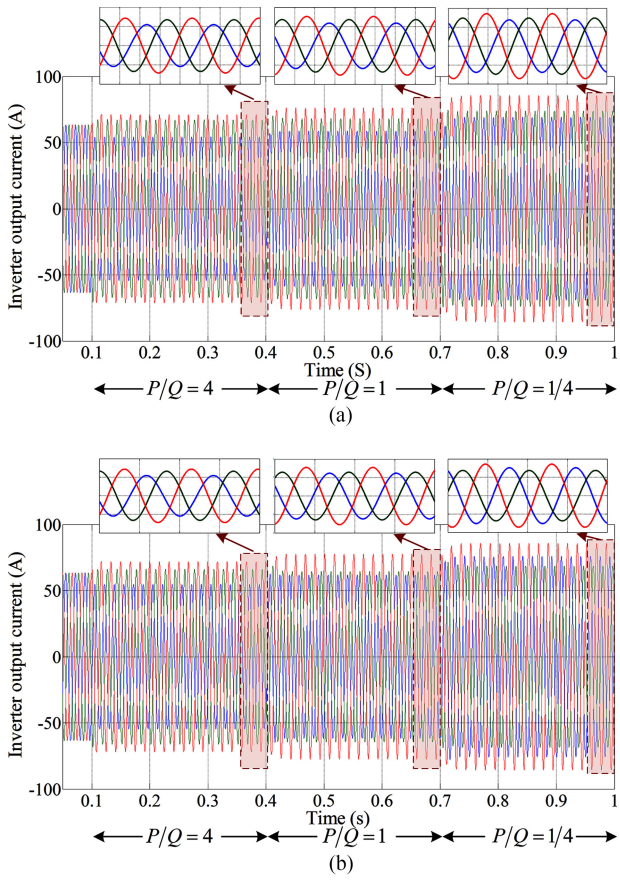

Fig. 9. Inverter output current in the weak resistive grid; (a) $\tilde{p}$-minimization, (b) inphase current compensation.

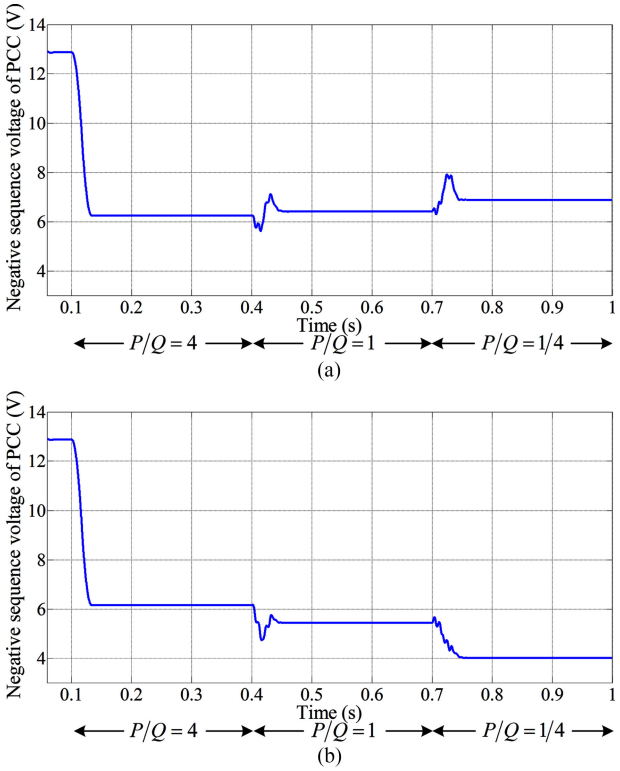

Fig. 10. Negative sequence voltage of PCC in the weak resistive grid; (a) $\tilde{p}$-minimization, (b) inphase current compensation.

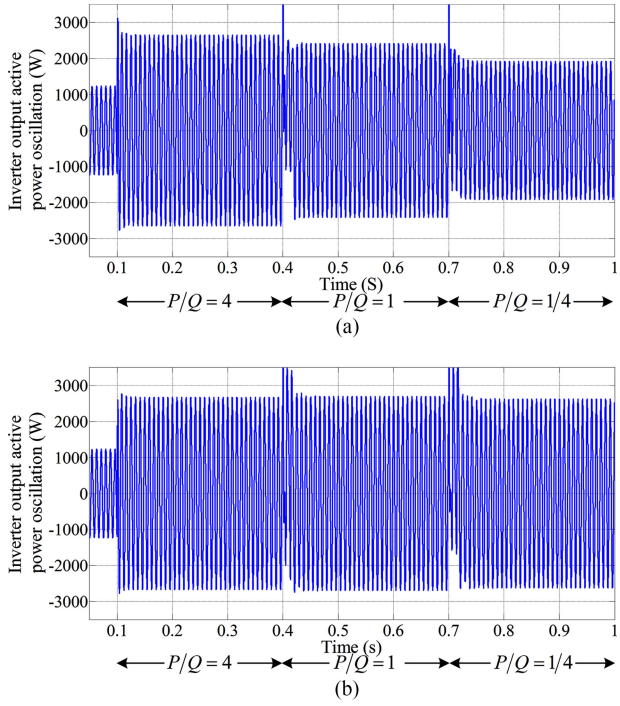

Fig. 11. Active power oscillations at the DG output in the weak resistive grid; (a) $\tilde{p}$-minimization, (b) inphase current compensation.

Fig. 6 shows the output current of DG in the inductive grid. The phasor diagrams of the DG output current are shown in Fig. 4. Fig. 7 shows the negative sequence voltage of PCC in the inductive grid. From this figure, it can be observed that the PCC negative sequence voltage is reduced in all DG's operating conditions, and the reduction level in the inphase current compensation strategy is more than the active power oscillation minimization strategy. Active power oscillations at the DG output is shown in Fig. 8, which proves that the active power oscillation minimization strategy leads to smaller active power oscillation in all operating conditions. However, the reduction is more obvious at high power factor operation conditions.

In Fig. 9, DG's output current in the resistive grid is shown, and its phasor diagrams are shown in Fig. 5. From negative sequence voltage of PCC shown in Fig. 10, it can be observed that although both control strategies reduce the negative sequence voltage, the reduction level of inphase current compensation strategy is more than the active power oscillation minimization strategy, which is more obvious at reactive power compensation operating condition. Similar to inductive grid, the active power oscillation minimization strategy minimizes the DG output power oscillation in all operating conditions, as shown in Fig. 11. However, at reactive power compensation operation, the reduction is more obvious.

B. Experimental Verification

To verify the effectiveness of the two proposed control strategies and the simulation results, experiments are conducted on a three-phase grid interfacing DG system prototype. The experimental setup parameters are shown in Table V, and the system is controlled by dSPACE 1103. The two proposed control strategies are tested under two grid conditions: 1) inductive grid ($X_{\rm Grid} = 1.88\ \Omega$ and $R_{\rm Grid} = 0.2\ \Omega$) with $|i^-_{\rm DG_{ref}}| = 2.5$ A, and 2) weak resistive grid ($X_{\rm Grid} = 0.94\ \Omega$ and $R_{\rm Grid} = 1.9\ \Omega$) with $|i^-_{\rm DG_{ref}}| = 1.5$ A. In each test, DG works with high power factor (large P/Q ratio; $P_{\rm ref} = 280$ W, $Q_{\rm ref} = 70$ VAR) and as a reactive power compensator (small P/Q ratio; $P_{\rm ref} = 70$ W, $Q_{\rm ref} = 280$ VAR). The results are shown in Figs. 12–15.

TABLE V
SYSTEM PARAMETERS FOR EXPERIMENTS

	Symbol	Value
DC-link voltage	$v_{\rm dc}$	150 V
Reference active power	$P_{\rm ref}$	280 W → 70 W
Reference reactive power	$Q_{\rm ref}$	70 Var → 280 Var
Three phase unbalance load	$R_{\rm Load}$	Three phase: 9Ω, 5Ω, 3Ω
Grid phase voltage (rms)	v_g	50 V
Grid frequency	f_g	60 Hz
Grid impedance	$Z_{\rm Grid}$	$X_{\rm Grid}$: 1.88 Ω → 0.94 Ω $R_{\rm Grid}$: 0.2 Ω → 1.9 Ω

In Figs. 12 and 13, the negative sequence voltage of PCC and DG's output active power oscillations in the inductive grid are shown, respectively. In these tests, the control strategy is switched from balance DG current injection without compensation strategy to the proposed control strategies. These experimental results are summarized in Table VI.

The experimental results for negative sequence voltage of PCC and the active power oscillation of DG in the resistive

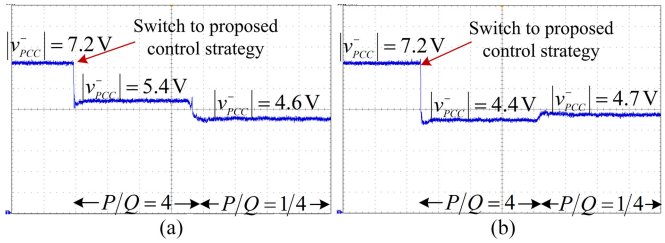

Fig. 12. Negative sequence voltage of PCC in the inductive grid $L_{\rm Grid} = 5$ mH and $R_{\rm Grid} = 0.2\ \Omega$; (a) $\tilde{p}$-minimization, (b) inphase current compensation strategy (time: 1 s/div, voltage: 1 V/div).

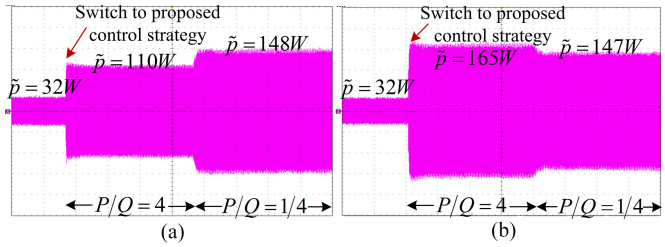

Fig. 13. Active power oscillations at the DG output in the inductive grid ($L_{\rm Grid} = 5$ mH and $R_{\rm Grid} = 0.2\ \Omega$); (a) $\tilde{p}$-minimization strategy, (b) inphase current compensation strategy (time: 1 s/div, power: 50W/div).

TABLE VI
SUMMARY OF EXPERIMENTAL RESULTS FOR TWO PROPOSED CONTROL STRATEGIES UNDER INDUCTIVE GRID AND WEAK GRID CONDITIONS, AND DIFFERENT DG'S OUTPUT ACTIVE–REACTIVE POWERS

Grid impedance conditions		Inductive grid $R = 0.2\ \Omega$; $X = 1.88\ \Omega$		Weak grid $R = 1.9\ \Omega$; $X = 0.94\ \Omega$	
DG's output active–reactive powers		280 W 70 Var	70 W 280 Var	280 W 70 Var	70 W 280 Var
$\lvert v^-_{\rm PCC}\rvert$	$\tilde{p}$-minimization	5.4	4.6	4	4.4
	Inphase current	4.4	4.7	4	3.4
	$\frac{\tilde{p}-\text{minimization}}{\text{inphase current}}$ ratio	1.22	0.98	1	1.29
$\tilde{p}$	$\tilde{p}$-minimization	110	148	75	62
	Inphase current	165	147	76	100
	$\frac{\tilde{p}-\text{minimization}}{\text{inphase current}}$ ratio	0.66	1.00	0.99	0.62

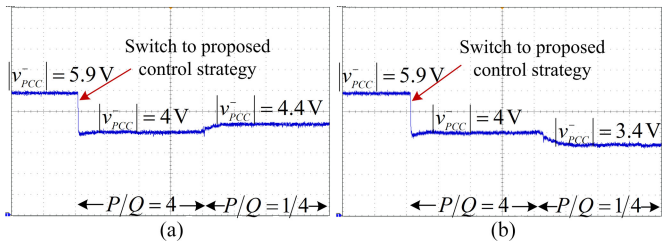

Fig. 14. Negative sequence voltage of PCC in the weak grid ($L_{\rm Grid} = 2.5$ mH and $R_{\rm Grid} = 1.9\ \Omega$); (a) $\tilde{p}$-minimization, (b) inphase current compensation strategy (time: 1 s/div, voltage: 1 V/div).

grid are shown in Figs. 14 and 15, respectively. Similar to inductive grid, in this test, the control strategy is switched from balance DG current injection without compensation strategy to the proposed control strategies. These results are summarized in Table VI.

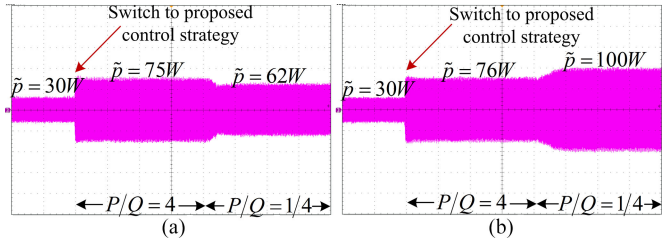

Fig. 15. Active power oscillations at the DG output in the weak grid ($L_{\rm Grid} = 2.5$ mH and $R_{\rm Grid} = 1.9\ \Omega$); (a) $\tilde{p}$-minimization strategy, (b) inphase current compensation strategy (time: 1 s/div, power: 50W/div)

Considering the experimental results and Table VI, it can be observed that utilizing the two proposed methods results in the grid unbalanced voltage compensation in which the compensation level of the inphase current compensation strategy is higher than the active power oscillation minimization strategy. Moreover, the active power oscillation minimization strategy minimizes the DG's output active power oscillation in each operation point. Similar to simulation results, the two proposed control strategies have the similar performance under inductive grid and DG works as a reactive power compensator ($P \ll Q$), or weak grid and DG works with high power factor ($P \gg Q$).

Considering aforementioned explanation, experimental results under different grid conditions and DG's output active–reactive powers verify the simulation results and discussions about control strategies and their performance.

VII. SUMMARY AND RECOMMENDATIONS

In Table VII, the previous discussions and comparisons are summarized, and appropriate control strategy under different grid conditions in terms of $X_{\rm Grid}/R_{\rm Grid}$ ratio and different DG's operating conditions in terms of P/Q ratio is recommended.

Considering Table VII, performance of the two proposed control strategies are similar to each other under three conditions: 1) In the normal inductive grid with large $X_{\rm Grid}/R_{\rm Grid}$ ratios and DG works as a reactive power compensator, 2) in the weak grid with $X_{\rm Grid}/R_{\rm Grid} \approx 1$ and DG works in different output active–reactive power ratios, or 3) in the weak grid with small $X_{\rm Grid}/R_{\rm Grid}$ ratios and DG works with high power factor. On the other hand, performances of the two methods are very different under the conditions of 1) normal inductive grid with large $X_{\rm Grid}/R_{\rm Grid}$ ratios and DG works with high power factor, or 2) weak grid with small $X_{\rm Grid}/R_{\rm Grid}$ ratios and DG works as a reactive power compensator. In this case, active power oscillation minimization or inphase current compensation method can be selected according to the objectives on power oscillation or PCC negative sequence voltage reduction.

Considering the size and capacity difference of DGs, different methods can be recommended also. In small DGs, due to low DG negative sequence current $|i^-_{\rm DG}|$, the difference of two proposed control strategies in terms of $|v^-_{\rm PCC}|$ reduction will not be very obvious. However, the active power oscillation minimization strategy provides minimum active power oscillation in each operation points. As a result, in small DG, if $|v^-_{\rm PCC}|$ reduction

TABLE VII
CONTROL STRATEGY RECOMMENDATION UNDER DIFFERENT GRID CONDITIONS AND DG'S OPERATING CONDITIONS

Grid impedance conditions		Large $X_{\mathrm{Grid}}/R_{\mathrm{Grid}}$ ratios		$X_{\mathrm{Grid}}/R_{\mathrm{Grid}} \approx 1$		Small $X_{\mathrm{Grid}}/R_{\mathrm{Grid}}$ ratios	
DG's output powers		$P \gg Q$	$P \ll Q$	$P \gg Q$	$P \ll Q$	$P \ll Q$	$P \gg Q$
$\tilde{p}$		$\tilde{p}_{\tilde{p}-\mathrm{min}} < \tilde{p}_{\mathrm{inphase}}$	$\tilde{p}_{\tilde{p}-\mathrm{min}} \approx \tilde{p}_{\mathrm{inphase}}$	$\tilde{p}_{\tilde{p}-\mathrm{min}} \approx \tilde{p}_{\mathrm{inphase}}$	$\tilde{p}_{\tilde{p}-\mathrm{min}} \approx \tilde{p}_{\mathrm{inphase}}$	$\tilde{p}_{\tilde{p}-\mathrm{min}} \approx \tilde{p}_{\mathrm{inphase}}$	$\tilde{p}_{\tilde{p}-\mathrm{min}} < \tilde{p}_{\mathrm{inphase}}$
$\tilde{q}$		$\tilde{q}_{\tilde{p}-\mathrm{min}} > \tilde{q}_{\mathrm{inphase}}$	$\tilde{q}_{\tilde{p}-\mathrm{min}} \approx \tilde{q}_{\mathrm{inphase}}$	$\tilde{q}_{\tilde{p}-\mathrm{min}} \approx \tilde{q}_{\mathrm{inphase}}$	$\tilde{q}_{\tilde{p}-\mathrm{min}} \approx \tilde{q}_{\mathrm{inphase}}$	$\tilde{p}_{\tilde{p}-\mathrm{min}} \approx \tilde{p}_{\mathrm{inphase}}$	$\tilde{q}_{\tilde{p}-\mathrm{min}} > \tilde{q}_{\mathrm{inphase}}$
$\lvert v_{\mathrm{PCC}}^{-}\rvert$		$\lvert v_{\mathrm{PCC}}^{-}\rvert_{\tilde{p}-\mathrm{min}} > \lvert v_{\mathrm{PCC}}^{-}\rvert_{\mathrm{inphase}}$	$\lvert v_{\mathrm{PCC}}^{-}\rvert_{\tilde{p}-\mathrm{min}} \approx \lvert v_{\mathrm{PCC}}^{-}\rvert_{\mathrm{inphase}}$	$\lvert v_{\mathrm{PCC}}^{-}\rvert_{\tilde{p}-\mathrm{min}} \approx \lvert v_{\mathrm{PCC}}^{-}\rvert_{\mathrm{inphase}}$	$\lvert v_{\mathrm{PCC}}^{-}\rvert_{\tilde{p}-\mathrm{min}} \approx \lvert v_{\mathrm{PCC}}^{-}\rvert_{\mathrm{inphase}}$	$\lvert v_{\mathrm{PCC}}^{-}\rvert_{\tilde{p}-\mathrm{min}} \approx \lvert v_{\mathrm{PCC}}^{-}\rvert_{\mathrm{inphase}}$	$\lvert v_{\mathrm{PCC}}^{-}\rvert_{\tilde{p}-\mathrm{min}} > \lvert v_{\mathrm{PCC}}^{-}\rvert_{\mathrm{inphase}}$
$\lvert i_{\mathrm{Grid}}^{-}\rvert$		$\lvert i_{\mathrm{Grid}}^{-}\rvert_{\tilde{p}-\mathrm{min}} > \lvert i_{\mathrm{Grid}}^{-}\rvert_{\mathrm{inphase}}$	$\lvert i_{\mathrm{Grid}}^{-}\rvert_{\tilde{p}-\mathrm{min}} \approx \lvert i_{\mathrm{Grid}}^{-}\rvert_{\mathrm{inphase}}$	$\lvert i_{\mathrm{Grid}}^{-}\rvert_{\tilde{p}-\mathrm{min}} \approx \lvert i_{\mathrm{Grid}}^{-}\rvert_{\mathrm{inphase}}$	$\lvert i_{\mathrm{Grid}}^{-}\rvert_{\tilde{p}-\mathrm{min}} \approx \lvert i_{\mathrm{Grid}}^{-}\rvert_{\mathrm{inphase}}$	$\lvert i_{\mathrm{Grid}}^{-}\rvert_{\tilde{p}-\mathrm{min}} \approx \lvert i_{\mathrm{Grid}}^{-}\rvert_{\mathrm{inphase}}$	$\lvert i_{\mathrm{Grid}}^{-}\rvert_{\tilde{p}-\mathrm{min}} > \lvert i_{\mathrm{Grid}}^{-}\rvert_{\mathrm{inphase}}$
Control Strategy Recommendation	$\tilde{p}$ is small	$\tilde{p}$-minimization	Both methods	Both methods	Both methods	Both methods	$\tilde{p}$-minimization
	$\tilde{q}$ is small	Inphase current	Both methods	Both methods	Both methods	Both methods	Inphase current
	$\lvert v_{\mathrm{PCC}}^{-}\rvert$ is small	Inphase current	Both methods	Both methods	Both methods	Both methods	Inphase current

is not the desired control parameter, active power oscillation minimization strategy is recommended.

In large DGs, due to possibility of high DG negative sequence current $|i_{\mathrm{DG}}^{-}|$, $|v_{\mathrm{PCC}}^{-}|$ can be obviously changed, and difference of the two proposed method in terms of $|v_{\mathrm{PCC}}^{-}|$ reduction will be more obvious. However, these two methods difference in terms of $\tilde{p}$ reduction may not be more obvious in comparison to small DG (as high $|i_{\mathrm{DG}}^{-}|$ tends to increase $\tilde{p}$ but low $|v_{\mathrm{PCC}}^{-}|$ tends to decrease $\tilde{p}$). As a result, in large DG, inphase current compensation strategy is recommended.

Finally, when multiple DGs participate in the unbalanced voltage compensation, active power oscillation minimization strategy may result in different DGs acting as virtual negative sequence impedances with different phase angles according to their active and reactive powers output. This will lead to negative sequence current circulation in the active power oscillation minimization strategy. However, the inphase current compensation method will guarantee that all DGs behave as negative sequence impedances with the same phase angle as the grid, resulting in zero negative sequence circulation current among DGs. Therefore, the inphase current compensation would be a good choice.

VIII. CONCLUSION

In this paper, two control strategies for three-phase power electronics interfaced DG systems are proposed in order to compensate the grid steady-state unbalanced voltage. In the first method, in order to reduce the adverse effects of compensation on the DGs' operation, DG's active power oscillation is minimized in the compensation strategy. In the second method, in order to effectively reduce the negative sequence voltage of the grid, DG's negative sequence current is set to be inphase with the grid negative sequence current. Both methods are based on the DG's equivalent negative sequence virtual impedance amplitude and phase angle control. From the analysis in this paper, the two methods have similar performance under 1) the normal inductive grid with large $X_{\mathrm{Grid}}/R_{\mathrm{Grid}}$ ratios and DG operates as reactive power compensator $(P \ll Q)$, 2) the weak grid with $X_{\mathrm{Grid}}/R_{\mathrm{Grid}} \approx 1$ and DG operates in different output active–reactive power ratios, or 3) the weak grid with small $X_{\mathrm{Grid}}/R_{\mathrm{Grid}}$ ratios and DG operates with high power factor $(P \gg Q)$. However, performance of the two methods in terms of power oscillations and the PCC negative sequence voltage reduction differs obviously under 1) the normal inductive grid with large $X_{\mathrm{Grid}}/R_{\mathrm{Grid}}$ ratios and DG is controlled with high power factor, or 2) the weak grid with small $X_{\mathrm{Grid}}/R_{\mathrm{Grid}}$ ratios and DG works as a reactive power compensator. Recommendations on how different methods are selected under various conditions are presented in this paper. Validity and effectiveness of the two proposed control strategies have been verified by simulations and experimental tests.

REFERENCES

[1] F. Nejabatkhah and Y.W. Li, "Overview of power management strategies of hybrid AC/DC microgrid," *IEEE Trans. Power Electron.*, vol. 30, no. 12, pp. 7072–7089, Dec. 2015.

[2] L. Tzung-Lin, H. Shang-Hung, and C. Yu-Hung, "D-STATCOM with positive-sequence admittance and negative-sequence conductance to mitigate voltage fluctuations in high-level penetration of distributed-generation systems," *IEEE Trans. Ind. Electron.*, vol. 60, no. 4, pp. 1417–1428, Apr. 2013.

[3] M. Savaghebi, A. Jalilian, J. C. Vasquez, and J. M. Guerrero, "Autonomous voltage unbalance compensation in an islanded droop-controlled microgrid," *IEEE Trans. Ind. Electron.*, vol. 60, no. 4, pp. 1390–1402, Apr. 2013.

[4] A. Camacho, M. Castilla, J. Miret, R. Guzman, and A. Borrell, "Reactive power control for distributed generation power plants to comply with voltage limits during grid faults," *IEEE Trans. Power Electron.*, vol. 29, no. 11, pp. 6224–6234, Nov. 2014.

[5] D. Graovac, V. A. Kati, and A. Rufer, "Power quality problems compensation with universal power quality conditioning system," *IEEE Trans. Power Del.*, vol. 22, no. 2, pp. 968–976, Apr. 2007.

[6] F. Barrero, S. Martínez, F. Yeves, F. Mur, and P. Martínez, "Universal and reconfigurable to UPS active power filter for line conditioning," *IEEE Trans. Power Del.*, vol. 18, no. 1, pp. 283–290, Jan. 2003.

[7] S. George and V. Agarwal, "A DSP-based optimal algorithm for shunt active filter under nonsinusoidal supply and unbalanced load conditions," *IEEE Trans. Power Electron.*, vol. 22, no. 2, pp. 593–601, Mar. 2007.

[8] B. Singh and J. Solanki, "An implementation of an adaptive control algorithm for a three-phase shunt active filter," *IEEE Trans. Ind. Electron.*, vol. 56, no. 8, pp. 2811–2820, Aug. 2009.

[9] F. Wang, J. L. Duarte, and M. A. M. Hendrix, "Grid-interfacing converter systems with enhanced voltage quality for microgrid application—Concept and implementation," *IEEE Trans. Power Electron.*, vol. 26, no. 12, pp. 3501–3513, Dec. 2011.

[10] J. M. Guerrero, P. C. Loh, T. L. Lee, and M. Chandorkar, "Advanced control architectures for intelligent microgrids—Part II: Power quality, energy storage, and AC/DC microgrids," *IEEE Trans. Ind. Electron.*, vol. 60, no. 4, pp. 1263–1270, Apr. 2013.

[11] J. Miret, A. Camacho, M. Castilla, L. G. Vicuna, and J. Matas, "Voltage support control strategies for static synchronous compensators under unbalanced voltage sags," *IEEE Trans. Ind. Electron.*, vol. 61, no. 2, pp. 808–820, Apr. 2013.

[12] J. Lu, F. Nejabatkhah, Y. Li, and B. Wu, "DG control strategies for grid voltage unbalance compensation," in *Proc. IEEE Energy Convers. Congr. Expo. Conf.*, Sep. 14–18, 2014, pp. 2932–2939.
[13] S. Chaudhary, R. Teodorescu, P. Rodriguez, P. Kjaer, and A. Gole, "Negative sequence current control in wind power plants with VSCHVDC connection," *IEEE Trans. Sustainable Energy*, vol. 3, no. 3, pp. 535–544, Jul. 2012.
[14] I. E. Otadui, U. Viscarret, M. Caballero, A. Rufer, and S. Bacha, "New optimized PWM VSC control structures and strategies under unbalanced voltage transients," *IEEE Trans. Ind. Electron.*, vol. 54, no. 5, pp. 2902–2914, Oct. 2007.
[15] A. Camacho, M. Castilla, J. Miret, A. Borrell, and L. de Vicuna, "Active and reactive power strategies with peak current limitation for distributed generation inverters during unbalanced grid faults," *IEEE Trans. Ind. Electron.*, vol. 62, no. 3, pp. 1515–1525, Mar. 2015.
[16] F. Wang, J. L. Duarte, and M. A. M. Hendrix, "Pliant active and reactive power control for grid-interactive converters under unbalanced voltage dips," *IEEE Trans. Power Electron.*, vol. 26, no. 5, pp. 1511–1521, May 2011.
[17] R. Teodorescu, M. Liserre, and P. Rodrıguez, *Grid Converters for Photovoltaic and Wind Power Systems*. New York, NY, USA: Wiley, 2011.
[18] J. Miret, M. Castilla, A. Camacho, L. Garcıa de Vicua, and J. Matas, "Control scheme for photovoltaic three-phase inverters to minimize peak currents during unbalanced grid-voltage sags," *IEEE Trans. Power Electron.*, vol. 27, no. 10, pp. 4262–4271, Oct. 2012.
[19] A. Camacho, M. Castilla, J. Miret, J. Vasquez, and E. Alarcon-Gallo, "Flexible voltage support control for three phase distributed generation inverters under grid fault," *IEEE Trans. Ind. Electron.*, vol. 60, no. 4, pp. 1429–1441, Apr. 2013.
[20] J. Miret, A. Camacho, M. Castilla, L.G. de Vicuna, and J. Matas, "Control scheme with voltage support capability for distributed generation inverters under voltage sags," *IEEE Trans. Power Electron.*, vol. 28, no. 11, pp. 5252–5263, Nov. 2013.
[21] C. T. Lee, C. W. Hsu, and P. T. Cheng, "A low-voltage ride-through technique for grid-connected converters of distributed energy resources," *IEEE Trans. Ind. Appl.*, vol. 47, no. 4, pp. 1821–1832, Jul. 2011.
[22] P. Rodriguez, A. Luna, J. Hermoso, I. E. Otadui, R. Teodorescu, and F. Blaabjerg, "Current control method for distributed generation power generation plants under grid fault conditions," in *Proc. IEEE 37th Annu. Conf. Ind. Electron. Soc.*, Nov. 2011, pp. 1262–1269.
[23] S. Alepuz, S. B. Monge, J. Bordonau, J. M. Velasco, C. Silva, J. Pont, and J. Rodriguez, "Control strategies based on symmetrical components for grid-connected converters under voltage dips," *IEEE Trans. Ind. Electron.*, vol. 56, no. 6, pp. 2162–2173, Jun. 2009.
[24] P. M. Andersson, *Analysis of Faulted Power Systems*. New York, NY, USA: IEEE Press, 1995.
[25] S. Boyd and L. Vandenberghe, *Convex Optimization*. New York, NY, USA: Cambridge Univ. Press, 2004.
[26] N. Hoffmann and F. W. Fuchs, "Minimal invasive equivalent grid impedance estimation in inductive–resistive power networks using extended Kalman filter," *IEEE Trans. Power Electron.*, vol. 29, no. 2, pp. 631–641, Feb. 2014.
[27] M. Liserre, F. Blaabjerg, and R. Teodorescu, "Grid impedance estimation via excitation of LCL-filter resonance," *IEEE Trans. Ind. App.*, vol. 43, no. 5, pp. 1401–1407, Sep./Oct. 2007.
[28] J. Huang, K. A. Corzine, and M. Belkhayat, "Small-signal impedance measurement of power-electronics-based AC power systems using line-to-line current injection," *IEEE Trans. Power Electron.*, vol. 24, no. 2, pp. 445–455, Sep. 2009.
[29] P. Rodriguez, J. Pou, J. Bergas, J. I. Candela, R.P. Burgos, and D. Boroyevich, "Decoupled double synchronous reference frame PLL for power converters controls," *IEEE Trans. Power Electron.*, vol. 22, no. 2, pp. 584–592, Mar. 2007.
[30] P. Roncero-Sanchez, X. del Toro Garcia, A. Parreno Torres, and V. Feliu, "Fundamental positive- and negative-sequence estimator for grid synchronization under highly disturbed operating conditions," *IEEE Trans. Power Electron.*, vol. 28, no. 8, pp. 3733–3746, Aug. 2013.
[31] P. Rodriguez, A. Luna, I. Candela, R. Mujal, R. Teodorescu, and F. Blaabjerg, "Multiresonant frequency-locked loop for grid synchronization of power converters under distorted grid conditions," *IEEE Trans. Ind. Electron.*, vol. 58, no. 1, pp. 127–138, Jan. 2011.
[32] A. Vidal, F. Freijedo, A. Yepes, P. Fernandez-Comesana, J. Malvar, O. Lopez, and J. Doval-Gandoy, "Assessment and optimization of the transient response of proportional-resonant current controllers for distributed power generation systems," *IEEE Trans. Ind. Electron.*, vol. 60, no. 4, pp. 1367–1383, Apr. 2013.

Farzam Nejabatkhah (S'09) received the B.Sc. (Hons.) and M.Sc. (Hons.) degrees in electrical engineering from the University of Tabriz, Tabriz, Iran, in 2009 and 2011, respectively. He is currently working toward the Ph.D. degree at the University of Alberta, Edmonton, AB, Canada.

His research interests include microgrid, power management, power quality, renewable energy and distributed generation, and power converter topologies and control.

Yun Wei Li (S'04–M'05–SM'11) received the B.Sc. in Engineering degree in electrical engineering from Tianjin University, Tianjin, China, in 2002, and the Ph.D. degree from Nanyang Technological University, Singapore, in 2006.

In 2005, he was a Visiting Scholar with Aalborg University, Aalborg, Denmark. From 2006 to 2007, he was a Postdoctoral Research Fellow at Ryerson University, Toronto, ON, Canada. In 2007, he was with Rockwell Automation Canada before he joined the University of Alberta, Edmonton, AB, Canada, in the same year. Since then, he has been at the University of Alberta, where he is currently a Professor. His research interests include distributed generation, microgrid, renewable energy, high-power converters and electric motor drives.

Dr. Li serves as an Associate Editor of the IEEE TRANSACTIONS ON POWER ELECTRONICS, the IEEE TRANSACTIONS ON INDUSTRIAL ELECTRONICS, and the IEEE JOURNAL OF EMERGING AND SELECTED TOPICS IN POWER ELECTRONICS. He received the Richard M. Bass Outstanding Young Power Electronics Engineer Award from the IEEE Power Electronics Society in 2013 and the Second Prize Paper Award of the IEEE Transactions on Power Electronics in 2014.

Bin Wu (S'89–M'92–SM'99–F'2008) received the M.A.Sc. and Ph.D. degrees in electrical and computer engineering from the University of Toronto, Toronto, ON, Canada, in 1989 and 1993, respectively.

He joined Ryerson University, Toronto, in 1993, where he is currently a Professor and the Senior NSERC/Rockwell Automation Industrial Research Chair in Power Electronics and Electric Drives. He has published more than 350 technical papers, authored/coauthored two Wiley-IEEE Press books, and holds more than 25 granted/pending US/European patents in the area of power conversion, medium voltage drives, and renewable energy systems.

Dr. Wu received the Gold Medal of the Governor General of Canada in 1993, the Premier's Research Excellence Award in 2001, the NSERC Synergy Award for Innovation in 2002, the Ryerson Distinguished Scholar Award in 2003, the Ryerson YSGS Outstanding Contribution to Graduate Education Award, and the Professional Engineers Ontario Engineering Excellence Medal in 2014. He is a Fellow of the Engineering Institute of Canada and the Canadian Academy of Engineering.